

NIR Counterparts to ULXs (III): Completing the photometric survey and selected spectroscopic results^{*}

K. M. López^{1,2†}, M. Heida^{3,4}, P. G. Jonker^{1,2}, M. A. P. Torres^{5,6,1}
T. P. Roberts⁷, D. J. Walton⁸, D.-S. Moon⁹, F. A. Harrison⁴

¹*SRON Netherlands Institute for Space Research, 3584 CA Utrecht, The Netherlands*

²*Department of Astrophysics/IMAPP, Radboud University, P.O. Box 9010, 6500 GL Nijmegen, The Netherlands*

³*European Southern Observatory, Karl-Schwarzschild-Straße 2, 85748 Garching bei München, Germany*

⁴*Space Radiation Laboratory, California Institute of Technology, Pasadena, CA 91125, USA*

⁵*Instituto de Astrofísica de Canarias, E-38200 La Laguna, Tenerife, Spain*

⁶*Departamento de Astrofísica, Universidad de La Laguna, Astrofísico Francisco Sánchez s/n, E-38206 La Laguna, Tenerife, Spain*

⁷*Centre for Extragalactic Astronomy, Department of Physics, University of Durham, South Road, Durham DH1 3LE, United Kingdom*

⁸*Institute of Astronomy, Cambridge University, Madingley Road, Cambridge CB3 0HA, United Kingdom*

⁹*Department of Astronomy and Astrophysics, University of Toronto, Toronto, ON M5S 3H4, Canada*

Accepted 2020 May 31. Received 2020 May 27; in original form 2019 October 29

ABSTRACT

We present results from the remaining sources in our search for near-infrared (NIR) candidate counterparts to ultraluminous X-ray sources (ULXs) within $\simeq 10$ Mpc. We observed 23 ULXs in 15 galaxies and detected NIR candidate counterparts to six of them. Two of these have an absolute magnitude consistent with a single red supergiant (RSG). Three counterparts are too bright for a RSG and spatially extended, and thus we classify them as stellar clusters. The other candidate is too faint for a RSG. Additionally, we present the results of our NIR spectroscopic follow-up of five sources: four originally classified as RSG and one as a stellar cluster on the basis of previous photometry. The stellar cluster candidate is actually a nebula. Of the four RSGs candidates, one source has a broad H α emission line redshifted by $\sim z = 1$, making it a background AGN. Two other sources show stellar spectra consistent with them being RSGs. The final RSG candidate is too faint to classify, but does not show strong (nebular) emission lines in its spectrum. After our search for NIR counterparts to 113 ULXs, where we detected a candidate counterpart for 38 ULXs, we have spectroscopically confirmed the nature of 12: five sources are nebulae, one source is not classified, one source is an AGN and five are RSGs. These possible five ULX-RSG binary systems would constitute $\simeq (4\pm 2)\%$ of the observed ULXs, a fraction almost four times larger than what was predicted by binary evolution simulations.

Key words: stars: black holes – infrared: stars – X-rays: individual: XMMU J024323.5+372038 – X-rays: individual: 2E 1402.4+5440 – X-rays: individual: RX J073655.7+653542 – X-rays: individual: CXOU J140314.3+541807

1 INTRODUCTION

Ever since their discovery in 1981 (Long et al. 1981), the nature of ultraluminous X-ray sources (ULXs) is puzzling, due to their high X-ray luminosities. ULXs are defined as point-like, off-nuclear sources with an X-ray luminosity $L_X > 10^{39}$ erg s⁻¹, i.e. larger than the Eddington luminosity for a

10 M $_{\odot}$ black hole (Kaaret et al. 2017). Several scenarios have been proposed to explain the high luminosities of these sources. A first scenario considers the possibility of a ULX being powered by a stellar-mass compact object either emitting anisotropically (King et al. 2001), or accreting at super-Eddington rates (Begelman 2002; Moon et al. 2003; Gladstone et al. 2009). Examples of the latter include the several neutron star (NS) ULXs discovered in the past 6 years (e.g. Bachetti et al. 2014; Fürst et al. 2016; Israel et al. 2017a,b; Carpano et al. 2018; Sathyaprakash et al. 2019; Rodríguez Castillo et al. 2019). These systems accrete from different

^{*} Based on observations made with ESO Telescopes at the La Silla Paranal Observatory under programme 0102.D-0529(A).

[†] Contact e-mail: K.M.Lopez@srn.nl

Table 1. Journal of the imaging observations presented in this manuscript.

Galaxy	Date observed	Effective exposure time ^a (sec)	Total exposure time ^b (sec)	Instrument/ Telescope	Band	WCS 1- σ uncertainty ^c (")	Average seeing (")	Distance (Mpc)	Distance reference
NGC 55	2018 October 22	5600	5600	SOFI/NTT	<i>H</i>	0.30	0.8	1.96 \pm 0.16	A
NGC 253*	2017 January 15	2920	3000	LIRIS/WHT	<i>H</i>	0.50	2.0	3.56 \pm 0.28	A
NGC 253	2018 October 20	5400	5500	SOFI/NTT	<i>H</i>	0.50	1.1	3.56 \pm 0.28	A
NGC 253	2018 October 21	5400	5500	SOFI/NTT	<i>H</i>	0.51	0.7	3.56 \pm 0.28	A
NGC 598	2018 October 21	5500	5500	SOFI/NTT	<i>H</i>	0.18	0.9	0.91 \pm 0.05	A
NGC 628*	2019 January 24	2550	2550	WIRC/Palomar	<i>K_s</i>	0.26	1.2	9.77 \pm 0.32	B
NGC 1291	2018 October 20	750	750	SOFI/NTT	<i>H</i>	0.19	0.6	9.08 \pm 0.29	B
NGC 1313	2018 October 22	5500	5500	SOFI/NTT	<i>H</i>	0.39	0.7	4.25 \pm 0.34	A
NGC 3623*	2018 January 25	3380	4000	LIRIS/WHT	<i>H</i>	0.28	1.2	12.19 \pm 2.44	A
NGC 3627*	2019 January 27	1910	2510	LIRIS/WHT	<i>H</i>	0.29	1.1	10.33 \pm 2.07	A
NGC 3628*	2018 January 27	3690	3500	LIRIS/WHT	<i>H</i>	0.20	1.3	10.30 \pm 2.06	A
NGC 4258*	2018 January 25	1860	3500	LIRIS/WHT	<i>H</i>	0.47	1.3	7.31 \pm 0.37	A
NGC 4258*	2019 January 24	3870	7350	WIRC/Palomar	<i>K_s</i>	0.46	1.6	7.31 \pm 0.37	A
NGC 4631*	2019 January 25	6630	7200	WIRC/Palomar	<i>K_s</i>	0.38	1.2	7.35 \pm 0.74	A
NGC 4594*	2019 January 24	1700	2000	LIRIS/WHT	<i>H</i>	0.20	1.3	11.27 \pm 1.35	A
NGC 5055*	2018 January 26	2000	2000	LIRIS/WHT	<i>H</i>	0.35	1.3	8.87 \pm 0.29	B
NGC 5194*	2017 January 14	2380	2500	LIRIS/WHT	<i>H</i>	0.77	1.2	9.05 \pm 0.24	C
NGC 5457	2019 January 24	3500	3500	LIRIS/WHT	<i>H</i>	0.26	0.9	6.95 \pm 0.42	A

Notes: ^a:Effective exposure time, not necessarily equal to the total exposure time^b (i.e., images taken during twilight, cloudy intervals were rejected and are not counted in the effective exposure time, whereas they are included in the total exposure time). ^c:Statistical uncertainty with respect to the reference catalog, given by the STARLINK GAIA tool. Objects marked with * indicate the images for which sky offsets with total time equal to that of the on-source time were taken. References: A: [Tully et al. \(2013\)](#), B: [McQuinn et al. \(2017\)](#) and C: [Tikhonov et al. \(2015\)](#).

types of stars, i.e. NGC 7793 P13, has a B9 supergiant donor ([Motch et al. 2011](#)); four NS ULXs most likely accrete from a young, massive main sequence star ([Bachetti et al. 2014](#); [Fürst et al. 2016](#); [Israel et al. 2017a,b](#); [Sathyaprakash et al. 2019](#); [Rodríguez Castillo et al. 2019](#)); and the remaining NS ULX was recently discovered to accrete from a RSG with an orbital period of 0.8 – 2.1 years ([Heida et al. 2019](#)).

The second scenario is that of a ULX powered by a BH more massive than 10 M_{\odot} (e.g. [Zampieri & Roberts 2009](#)), which owing to its higher Eddington luminosity, accretes at or below the Eddington limit. The existence of these more massive BHs was proven by the detection of gravitational waves (e.g. [Abbott et al. 2016a,b](#); [The LIGO Scientific Collaboration et al. 2018](#)), with BH masses between 10 M_{\odot} and 80 M_{\odot} . In a third scenario, the ULX harbors a BH more massive than the systems discussed before, but less massive than the super-massive BHs in the centre of massive galaxies ([Kormendy & Ho 2013](#)). These intermediate systems, with masses between 10^2 and $10^5 M_{\odot}$, are called intermediate mass black holes (IMBHs) and they would accrete at sub-Eddington rates (e.g. [Jonker et al. 2010](#); [Farrell et al. 2011](#); [Mezcua et al. 2013](#); [Heida et al. 2015b](#); [Earnshaw 2016](#)).

The only ULXs for which we have reliable accretor mass constraints are the pulsars, which must contain neutron stars and therefore accretors with $M < 3 M_{\odot}$ ([Kalogera & Baym 1996](#)). Apart from the detection of pulsations, a way to identify the nature of the accretor powering the ULXs is dynamical mass measurements. Detecting the donor star is the first step (e.g. [Patruno & Zampieri 2008](#); [Heida et al. 2016](#); [Vinokurov et al. 2018](#); [Qiu et al. 2019](#)), as subsequent spectroscopic observations can be used to constrain the radial velocity amplitude of the donor star, and hence, the compact object mass function (e.g. [Motch et al. 2014](#)). See [Casares & Jonker 2014](#) for a detailed description of the application of this dynamical method to X-ray binaries.

Multi-wavelength searches for the donor stars have been pursued for more than a decade. Some have observed ULXs in the optical range (e.g. [Ptak et al. 2006](#); [Gutiérrez & López-Corredoira 2006](#); [Roberts et al. 2011](#); [Gladstone et al. 2013](#); [Fabrika et al. 2015](#)). As several of the ULXs are located in or near young star clusters (e.g. [Fabbiano et al. 2001](#); [Roberts et al. 2002](#); [Poutanen et al. 2013](#)), some donor stars of ULXs might as well be red supergiants (RSGs, [Copperwheat et al. 2005, 2007](#); [Patruno & Zampieri 2008](#)), which are bright in the near-infrared (NIR) band. In light of this, we started an observing campaign of ULXs in the NIR ([Heida et al. 2014](#); [López et al. 2017](#)), tailored to detect RSG donor stars ($-8 < H, K_s < -11$, [Elias et al. 1985](#); [Drilling & Landolt 2000](#)). We targeted sources at distances up to 10 Mpc, within uncertainties. Of the 97 ULXs observed by [Heida et al. \(2014\)](#) and [López et al. \(2017\)](#), we detected a NIR candidate counterpart for 33 ULXs. Of these 33 NIR sources, 19 had the absolute magnitude consistent with a RSG. So far, we performed spectroscopic follow-up observations for seven out of these 19 candidate RSGs and confirmed the RSG nature for three counterparts: ULX RX J004722.4-252051 (in NGC 253, [Heida et al. 2015a](#)), ULX J022721+333500 (in NGC 925) and ULX J120922+295559 (in NGC 4136, [Heida et al. 2016](#)). Additionally, we discovered that four counterparts, initially classified as RSG based on photometry, are actually nebulae partially powered by the X-ray emission of the ULX: ULX J022727+333443 (in NGC 925), ULX J120922+295551 (in NGC 4136), ULX Ho II X-1 (in Holmberg II, [Heida et al. 2016](#)) and [SST2011] J110545.62+000016.2 (in NGC 3521, [López et al. 2019](#)). This means that, at the time of writing this manuscript, the photometric and spectroscopic observations provided three confirmed RSGs, 12 candidate RSGs, four confirmed nebulae and 14 candidate stellar clusters/AGNs. Recently, [Lau et al. \(2019\)](#) observed 96 ULX within 10 Mpc in the mid-IR

Table 2. Complete sample of the 23 ULXs for which we took images in either H - or K_s -band.

Galaxy	ULX name (SIMBAD [†])	X-ray positional		X-ray position uncertainty ^a (")	X-ray position reference	Positional uncertainty ^b (")
		R.A. (hh:mm:ss)	Dec (dd:mm:ss)			
NGC 55	[BWE2015] NGC 55 119	00:15:28.9	−39:13:18.8	0.5	Liu (2011)	1.7
NGC 253	[WMR2006] NGC 253 XMM7	00:47:09.2	−25:21:23.3	0.2	Lin et al. (2012)	1.6
NGC 253	RX J004717.4-251811	00:47:17.60	−25:18:11.00	0.33	Colbert et al. (2004)	1.8
NGC 253	[WMR2006] NGC 253 XMM4	00:47:23.5	−25:19:04.2	0.2	Lin et al. (2012)	1.6
NGC 253	2XMM J004820.0-251010	00:48:20.1	−25:10:10.3	0.4	Lin et al. (2012)	1.9
NGC 598	ChASem33 J013350.89+303936.6	01:33:50.9	30:39:36.8	0.5	Liu (2011)	1.6
NGC 628*	[KKG2005] M74 X-1	01:36:51.1	15:45:46.8	0.5	Liu (2011)	2.7
NGC 1291	CXO J031718.9-410627	03:17:18.54	−41:06:29.26	0.29	This work	1.0
NGC 1313	NGC 1313 X-2	03:18:22.27	−66:36:03.72	0.23	This work	1.4
NGC 3623*	CXO J111858.4+130530	11:18:58.5	13:05:30.9	0.5	Liu (2011)	1.7
NGC 3627*	[SST2011] J112020.90+125846.6	11:20:20.9	12:58:46.0	0.5	Liu (2011)	1.7
NGC 3628*	CXOU J112037.3+133429	11:20:37.37	3:34:29.02	0.23	This work	0.9
NGC 4258	[CHP2004] J121854.5+471649	12:18:54.50	47:16:49.00	0.33	Colbert et al. (2004)	1.7
NGC 4258	[CHP2004] J121855.8+471759	12:18:55.73	47:17:59.17	0.33	Wang et al. (2016)	1.7
NGC 4258	[CHP2004] J121856.4+472126	12:18:56.42	47:21:26.70	0.47	Colbert et al. (2004)	2.0
NGC 4258	CXO J121903.84+471832.4	12:19:03.87	47:18:32.29	0.33	Wang et al. (2016)	1.7
NGC 4594	[LB2005] NGC 4594 ULX2	12:39:48.62	−11:37:13.10	0.47	Li et al. (2010)	1.5
NGC 4631**	[SST2011] J124155.56+323216.9	12:41:55.57	32:32:16.87	0.47	Mineo et al. (2012)	1.8
NGC 4631**	CXO J124157.4+323202	12:41:57.42	32:32:02.98	0.47	Mineo et al. (2012)	1.8
NGC 4631**	[WMR2006] NGC4631 XMM3	12:41:58.03	32:28:51.56	0.33	Wang et al. (2016)	1.5
NGC 5055	[SST2011] J131519.54+420302.3	13:15:19.55	42:03:02.30	0.47	Swartz et al. (2004)	1.8
NGC 5194	[CHP2004] J132940.0+471237	13:29:40.0	47:12:36.9	0.5	Liu (2011)	2.8
NGC 5457	2XMM J140228.3+541625	14:02:28.30	54:16:26.69	0.47	Mineo et al. (2012)	1.6

Notes: ^a1- σ uncertainty. ^b99.7% (3- σ) confidence radius of the position of the ULX within which we search for counterparts; this value is calculated adding the uncertainties of the astrometric correction on the NIR images (see Table 1) and the uncertainties of the X-ray position. We added systematic uncertainties linearly and statistical uncertainties quadratically. [†]Set of Identifications, Measurements and Bibliography for Astronomical Data (SIMBAD; Wenger et al. 2000). Sources analyzed by *Heida et al. (2014) and by **López et al. (2017), that we re-observe to provide deeper images with better seeing.

Table 3. Log of the Keck/MOSFIRE spectroscopic observations. Apparent and absolute H -band magnitudes from Heida et al. (2014) and López et al. (2017) are provided.

Galaxy	ULX	H (mag)	M_H (mag)	Observation date	Filter	Time on source (h)	P.A. (deg)
NGC 1058	XMMU J024323.5+372038	19.7 ± 0.4	−10.1 ± 0.4	2019 January 17	J	2.4	0
NGC 2403	RX J073655.7+653542	17.46 ± 0.02	−10.05 ± 0.26	2019 January 17	J	0.4	37
NGC 5457	2E 1402.4+5440	19.3 ± 0.2	−9.9 ± 0.2	2019 May 23	H	2.4	35
NGC 5457	[LB2005] NGC 5457 X26*	17.78 ± 0.01	−11.44 ± 0.22	2019 May 23	H	2.4	35
NGC 5457	CXOU J140314.3+541807	18.35 ± 0.10	−10.69 ± 0.10	2019 July 23	H	1.0	50

*Source originally classified as a stellar cluster. In our multi-object spectroscopic observations we took a spectrum of this source at the same time as the spectrum of 2E 1402.4+5440 was obtained as it was in the field of view.

with the *Spitzer Space Telescope*. They detected identified 12 ULXs with candidate counterparts whose absolute mid-IR magnitude is consistent with being RSGs.

In this manuscript we present the final results of our imaging campaign as well as results of our spectroscopic follow-up with Keck/MOSFIRE of four candidate RSGs identified earlier in our campaigns by Heida et al. (2014) and López et al. (2017). We describe the observed sample in Section 2, the NIR (imaging and spectral) observations in Section 3 and data reduction/photometry in Section 4. Our results are presented and discussed in Section 5. We sum-

marize the results of the 8-year-long systematic photometric search in Section 6 and we end with the conclusions of our work in Section 7.

2 SAMPLE

For our imaging observations, our sample consists of 23 ULXs located in 15 different galaxies within 10 Mpc from our Galaxy (see Table 1). This sample completes the NIR imaging campaign started by Heida et al. (2014) and contin-

ued by López et al. (2017). Four ULXs were observed before by Heida et al. (2014) and three ULXs were observed before by López et al. (2017), but we observe them again under better sky conditions to make the survey as homogeneous in depth as possible. Several of the sources were originally discovered with the *Röntgensatellit* (*ROSAT*), three sources ([WMR2006] NGC253 XMM7, [WMR2006] NGC253 XMM4 and 2XMM J004820.0-251010) have been re-observed by the X-ray Multi-Mirror Mission (*XMM-Newton*) and the rest by the *Chandra* X-ray Observatory, offering an improved X-ray position (see Table 2). Note that we report the $3\text{-}\sigma$ confidence radius of the position of the ULX which takes into account the X-ray positional uncertainty of the ULX and the WCS uncertainty of the NIR image (see Section 4.1).

Additionally, we obtain NIR spectra of five ULX candidate counterparts (see Table 3). Three sources (XMMU J024323.5+372038 in NGC 1058, and 2E 1402.4+5440 and CXOU J140314.3+541807 in NGC 5457) were photometrically identified and classified by Heida et al. (2014) as potential RSGs. The remaining two sources were photometrically identified and classified by López et al. (2017): one as a potential RSG (RX J073655.7+653542 in NGC 2403) and one as a stellar cluster ([LB2005] NGC 5457 X26). The latter is located in the field of view from the ULX 2E 1402.4+5440.

3 OBSERVATIONS

3.1 NIR Imaging

H-band images of regions of galaxies containing ULXs were obtained with the Long-slit Intermediate Resolution Infrared Spectrograph (LIRIS, Manchado et al. 1998) mounted on the 4.2-m William Herschel Telescope (WHT) and the Son OF Isaac (SOFI, Moorwood et al. 1998) mounted on the 3.6-m New Technology Telescope (NTT); whereas *K_s*-band imaging was obtained with the Wide Field Infrared Camera (WIRC) mounted on the Palomar Hale 5-m Telescope. LIRIS has a field of view of $4.27' \times 4.27'$ and a pixel scale of $0.25''$ /pixel. SOFI has a field of view of $4.92' \times 4.92'$ and a pixel scale of $0.288''$ /pixel and WIRC has a field of view of $8.7' \times 8.7'$ and a pixel scale of $0.2487''$ /pixel.

The LIRIS observations were performed using 7 or 8 repetitions of a 5-point dither pattern where 5 images (10 or 20 seconds exposure per image) were taken at each point. For the observations done with SOFI, we used the template SOFLimg_obs_AutoJitter, in which an observing cycle of 10 images (5 or 10 seconds exposure per image) is repeated 55 (or 110) times. The WIRC observations consisted of a 5-point dither pattern where 6 images of 5 seconds exposure each were taken at each point. This pattern was repeated 17 times for NGC 628, 48 times for NGC 4631 and 49 times for NGC 4258. Sky offsets were taken if the field of view was crowded (see Table 1, where we also indicate the filter and instrument/telescope used, the average seeing during the observation and the distance to each galaxy).

3.2 NIR Spectra

We obtained *J*- and/or *H*-band spectroscopy of five ULX counterparts with the Multi-Object Spectrometer for Infra-Red Exploration (MOSFIRE, McLean et al. 2010, 2012),

Table 4. The ULX NIR candidate counterparts for which we analysed archival *HST* observations.

ULX name	<i>HST</i> obs. ID	Filter
2XMM J004820.0-251010	10915	ACS/WFC/F606W ACS/WFC/F814W
NGC 1313 X-2	14057	WFC3/UVIS/F555W WFC3/UVIS/F814W
RX J073655.7+653542	11719	WFC3/IR/F125W WFC3/IR/F110W
CXOU J140314.3+541807	9490	WFC3/IR/F160W ACS/WFC/F555W ACS/WFC/F814W

mounted on the 10-m Keck I telescope on Mauna Kea. MOSFIRE has a field of view of $6.1' \times 6.1'$, a pixel scale of $0.18''$ /pixel and a robotic slit mask system with 46 reconfigurable slits. XMMU J024323.5+372038 and RX J073655.7+653542 were observed on 2019 January 17 with an $0.7''$ slit in the *J*-band, with seeing varying between $0.4 - 0.7''$. The ULXs in NGC 5457 were observed with an $0.7''$ slit in the *H*-band; 2E 1402.4+5440 and [LB2005] NGC 5457 X26 on 2019 May 23 with a seeing of $\sim 0.5''$, and CXOU J140314.3+541807 on 2019 July 13 with a seeing of $\sim 0.8''$. For all sources we used an ABBA nodding pattern with a nod amplitude along the slit chosen to avoid nearby sources. The integration time per exposure was 119.3 s for all observations. The spectral resolution *R* and spectral coverage $\Delta\lambda$ for the *J*-band observation are $R = 3100$ and $\Delta\lambda = 11530 - 13520 \text{ \AA}$; for the *H*-band observations, $R = 3660$ and $\Delta\lambda = 14500 - 18220 \text{ \AA}$. The total exposure times are listed in Table 3. We observed A0V-type telluric standard stars at similar airmass as the science targets before and after every series of exposures. These were also used for flux calibration. For every slit mask configuration, we obtained flat-field and comparison lamp spectra in the afternoon before the observing night.

4 DATA REDUCTION

4.1 NIR Imaging

The data reduction was performed using the THELI pipeline (Schirmer 2013). To flat-field correct the NIR data, THELI produces a master flat by median combining sky images taken during twilight. Then, median combining the data frames without correcting for the offsets introduced by the dithering, it generates a sky background model which is subtracted from each individual image. After this, THELI detects sources in each image using SExtractor (Bertin & Arnouts 1996) and matches them to sources from the 2 Micron All Sky Survey (2MASS; Skrutskie et al. 2006) with SCAMP (Bertin 2006). This creates an astrometric solution which then is used for the coaddition of all the data frames using SWARP (Bertin et al. 2002).

We improved the accuracy of the global astrometric solution of the coadded NIR images using the STARLINK tool GAIA, fitting several isolated point sources from Gaia Data

Table 5. NIR candidate counterparts to the ULXs listed in Table 2 and our preliminary classification as candidate RSG, stellar cluster (SC) or (N/A) without classification. The preliminary classification is based on their absolute magnitude, WISE colours, visual inspection of the NIR image and/or spatial extent of the candidate counterpart.

Galaxy	ULX name	R.A	Dec.	Positional ^a uncertainty ($''$)	Filter	Apparent magnitude (mag)	Absolute ^b magnitude (mag)	Preliminary classification
		(hh:mm:ss)	(dd:mm:ss)					
NGC 55	[BWE2015] NGC 55 119	–	–	–	<i>H</i>	> 20.5	> –5.9	–
NGC 253	[WMR2006] NGC 253 XMM7	–	–	–	<i>H</i>	> 18.7	> –9.4	–
NGC 253	RX J004717.4 – 251811	–	–	–	<i>H</i>	> 17.3	> –10.8	–
NGC 253	[WMR2006] NGC 253 XMM4	–	–	–	<i>H</i>	> 16.1	> –12.0	–
NGC 253	2XMM J004820.0 – 251010	00:48:19.9	–25:10:10.3	1.6	<i>H</i>	20.4 ± 0.1	–7.4 ± 0.2	N/A
NGC 598	ChASeM33 J013350.89 + 303936.6	01:33:50.9	+30:39:36.6	0.6	<i>H</i>	11.8 ± 0.1	–13.0 ± 0.1	SC
NGC 628	[KKG2005] M74 X-1	–	–	–	<i>K_s</i>	> 19.5	> –10.4	–
NGC 1291	CXO J031718.9 – 410627	03:17:18.6	–41:06:28.9	0.6	<i>H</i>	11.3 ± 0.1	–18.4 ± 0.1	SC
NGC 1313	NGC 1313 X-2	03:18:22.4	–66:36:04.0	1.2	<i>H</i>	21.1 ± 0.2	–7.1 ± 0.2	RSG
NGC 3623	CXO J111858.4 + 130530	–	–	–	<i>H</i>	> 18.9	> –11.5	–
NGC 3627	[SST2011] J112020.90 + 125846.6	–	–	–	<i>H</i>	> 19.0	> –11.1	–
NGC 3628	CXOU J112037.3 + 133429	11:20:37.3	+13:34:28.9	0.7	<i>H</i>	20.4 ± 0.2	–9.7 ± 0.5	RSG
NGC 4258	[CHP2004] J121854.5 + 471649	–	–	–	<i>H</i>	> 19.6	> –9.7	–
NGC 4258	[CHP2004] J121855.8 + 471759	–	–	–	<i>H</i>	> 18.2	> –11.1	–
NGC 4258	[CHP2004] J121856.4 + 472126	–	–	–	<i>K_s</i>	> 19.5	> –9.8	–
NGC 4258	CXO J121903.84 + 471832.4	–	–	–	<i>H</i>	> 19.0	> –10.3	–
NGC 4594	[LB2005] NGC 4594 ULX2	–	–	–	<i>H</i>	> 19.3	> –10.9	–
NGC 4631	[SST2011] J124155.56 + 323216.9	–	–	–	<i>K_s</i>	> 18.8	> –10.5	–
NGC 4631	CXO J124157.4 + 323202	–	–	–	<i>K_s</i>	> 17.9	> –11.4	–
NGC 4631	[WMR2006] NGC4631 XMM3	–	–	–	<i>K_s</i>	> 20.1	> –9.2	–
NGC 5055	[SST2011] J131519.54 + 420302.3	–	–	–	<i>H</i>	> 20.1	> –9.6	–
NGC 5194	[CHP2004] J132940.0 + 471237	–	–	–	<i>H</i>	> 19.8	> –10.0	–
NGC 5457	2XMM J140228.3 + 541625	14:02:28.2	+54:16:26.3	0.8	<i>H</i>	16.0 ± 0.1	–13.2 ± 0.1	SC

Notes: ^a:99.7% ($3\text{-}\sigma$) confidence radius of the position of the NIR candidate counterpart; this value is calculated taking into account the uncertainties of the astrometric correction on the NIR images and the uncertainties given by the source detection by SExtractor. We added systematic uncertainties linearly and statistical uncertainties quadratically. ^b:Values calculated using the distance from Table 1 and the apparent magnitude, with a $1\text{-}\sigma$ uncertainty.

Release 2 (DR2, Gaia Collaboration et al. 2018). We only used stars with a proper motion $\text{pm} < 5 \text{ mas yr}^{-1}$ to build a local astrometric solution around the position of the ULX. The rms errors of these fits are listed in Table 1, indicated as WCS (World Coordinate System) uncertainties.

4.2 NIR Spectra

We reduced the MOSFIRE spectra with the MOSFIRE data reduction pipeline (version 2018)¹. The pipeline outputs co-added, rectified 2D-spectra that are wavelength calibrated with an RMS $< 0.1 \text{ \AA}$. We used the FIGARO package (Shortridge 1993) to optimally extract the spectra and the MOLECFIT software (Kausch et al. 2015; Smette et al. 2015) to correct for telluric absorption. With MOLECFIT, we performed fits of regions with strong telluric features in the high signal-to-noise ratio (S/N) spectra of our A0V telluric standard stars to determine the atmospheric conditions and used those solutions to correct the science spectra, only fitting for the local continuum and correcting for changes in airmass. We used the same A0V telluric standards to correct for the instrument response and to provide an approximate flux calibration. We did not correct for slit losses, but expect

these to be small as our slit width matched or exceeded the seeing during most of our observations.

4.3 Photometry

4.3.1 NIR images

We performed aperture photometry to determine instrumental magnitudes. We used SExtractor for the source detection and photometry, making sure that each detection was more than $3\text{-}\sigma$ above the local background. As the aperture radius, we use the average full-width at half maximum (FWHM) of the point-like objects in each image determined with the STARLINK tool GAIA. Instrumental magnitudes for all detected sources were converted to apparent magnitudes using photometric zero points that we measured using isolated 2MASS objects in the field of view. Then, we determined the absolute magnitudes of candidate counterparts to ULXs using the distances given in Table 1. The ($1\text{-}\sigma$) uncertainties on these values are estimated taking into account the distance uncertainty, the uncertainty in the determination of the zero point magnitude and the uncertainty in the instrumental magnitude given by SExtractor. For the images in which we did not detect a counterpart, we estimated the limiting magnitude by simulating 10,000 stars at the

¹ <https://github.com/Keck-DataReductionPipelines/MosfireDRP>

position of the ULX using the IRAF² task MKOBJECTS and then detecting them with the task DAOFIND. Our limiting magnitude is the magnitude at which 99.7% of the simulated stars are detected.

4.3.2 *HST* images

For the four sources for which we analyse archival *HST* data (see Table 4), we also improved the accuracy of the astrometry using the STARLINK tool GAIA and isolated Gaia DR2 sources. Additionally, we performed aperture photometry on these *HST* images with SEXTRACTOR. To derive the magnitude we transform the instrumental magnitudes into apparent magnitudes using the VEGAMAG zero points of the corresponding *HST* filter as advised by Sirianni et al. (2005) and Kalirai et al. (2009). To correct for extinction on these data, we assumed $R_V = 3.1$ (Fitzpatrick 1999), $R_R = 2.31$, $R_I = 1.71$, $R_J = 0.72$, $R_H = 0.306$ (Yuan et al. 2013) and $N_H = 1.87 \times 10^{21}$ atoms cm^{-2} $\text{mag}^{-1} A_V$ (Bohlin et al. 1978).

4.4 X-ray astrometry

For all the ULXs in our sample accurate positions exist in the literature (see Table 2). However, we were able to improve the accuracy of the positions of 3 ULXs (CXO J031718.9-410627, NGC 1313 X-2 and CXOU J112037.3+133429) using archival Chandra/ACIS observations. For CXO J031718.9-410627 we used observation ID 2059, for NGC 1313 X-2 we used observation ID 4750 and for CXOU J112037.3+133429 we used observation ID 2919.

We used the task ACIS-PROCESS-EVENTS in CIAO (Dobrzycki et al. 1999) to reprocess the event files with the calibration files (CALDB version 4.9.0) taking into account whether the observations were made in the "Faint" or "Very Faint" mode. We then produced images from data in the 0.3 – 7 keV energy range, on which we run the WAVDETECT task (Dobrzycki et al. 1999) to establish accurate positions of all X-ray sources in the field of view of the Chandra ACIS CCDs. With this procedure we improved the X-ray position of ULXs NGC 1313 X-2 and CXOU J112037.3+133429 (see Table 2).

For the ULX in NGC 1291, CXO J031718.9-410627, we were able to further improve the knowledge of the location of the source by applying a boresight correction (e.g. Jonker et al. 2010; López et al. 2017). For this, we select only X-ray sources detected with more than 20 X-ray counts and that lie within 3' of the optical axis of the satellite. When found, we investigated whether counterparts in the Gaia DR2 catalogue exist. We take the Gaia DR2 source as a counterpart if it lies within 1'' from the position of the X-ray source. Subsequently, we determine the offsets between the RA and Dec. of the new and old source and we then apply shifts in RA and Dec. to the X-ray coordinates using the WCS-UPDATE tool. The updated coordinates are indicated in Table 2.

² IRAF is distributed by the National Optical Astronomy Observatories, which are operated by the Association of Universities for Research in Astronomy, Inc., under cooperative agreement with the National Science Foundation.

5 RESULTS AND DISCUSSION

Of the 23 ULXs we observed, we detect a NIR candidate counterpart for six of them (about 30%). Their apparent and absolute magnitudes are detailed in Table 5. For the cases where no counterpart is detected, the apparent (absolute) limiting magnitude of the NIR image at the position of the ULX is indicated, and it ranges from 16.1 to 20.5 (–12.0 to –5.9) mag.

Out of the six NIR candidate counterparts, three have absolute magnitudes in the *H*-band from -13.0 ± 0.1 to -18.4 ± 0.1 , i.e. too bright to be a single star. Hence, these sources are most likely unresolved groups of stars, perhaps a cluster of stars. Even though we do not know whether these clusters are gravitationally bound, i.e. whether they are stellar clusters, we do refer to them this way. One source is too faint to be a RSG so we do not give any classification to it. The remaining two sources have absolute magnitudes in the *H*, *K_s* consistent with those of a RSG, within uncertainties (Elias et al. 1985; Drilling & Landolt 2000). Below we discuss in detail each of the detected counterparts, providing some clues on their possible nature, based on their photometry and their spatial properties.

On the other hand, of our five sources spectroscopically observed, we confirm two RSG candidates as RSGs based on their stellar spectra and we reveal one RSG candidate to be an AGN. The SC candidate turns out to be a nebula and the last RSG candidate cannot be classified based on its spectrum, as no significant absorption or emission lines were detected.

5.1 NIR Red supergiant candidates

5.1.1 *NGC 1313 X-2*

This ULX has been observed several times, both in X-ray and in the optical (e.g. Stocke et al. 1995; Zampieri et al. 2004; Mucciarelli et al. 2005; Liu et al. 2007). It is now one of the six NS ULX on the basis of the detection of pulsations (Sathyaprakash et al. 2019). Zampieri et al. (2004) first identified an optical counterpart for this source and classified it as an evolved OB supergiant. On the other hand, Mucciarelli et al. (2005) resolved this counterpart into two sources (0.75'' apart) and classified them as a B0-O9 main sequence star and a G supergiant. Moreover, they concluded that NGC 1313 X-2 could be associated with either one of them. While Ramsey et al. (2006) identified the B type star as the counterpart to the ULX using *HST* data, Liu et al. (2007) argued that the spectral type of the counterpart is actually O7V. Additionally, they found a third source within the $1 - \sigma$ confidence radius that was then ruled out as a cosmic ray. Although this source has been spectroscopically followed-up, no radial velocity measurement or mass function has been established (see Pakull et al. 2006; Grisé et al. 2009; Roberts et al. 2011.) In fact, it was suggested that the optical emission may not come from the counterpart, but from the accretion disk (Roberts et al. 2011). We analyse the archival *HST* images of this source in the F555W, F814W and F125W filters. At the position of the ULX, we detect the two sources reported by Mucciarelli et al. (2005) (see Figure 1b). Their apparent, absolute Vega magnitudes and extinction are indicated in Table 6 and from them, we can see that the source labeled B has absolute *V*-, *I*- and *J*-band

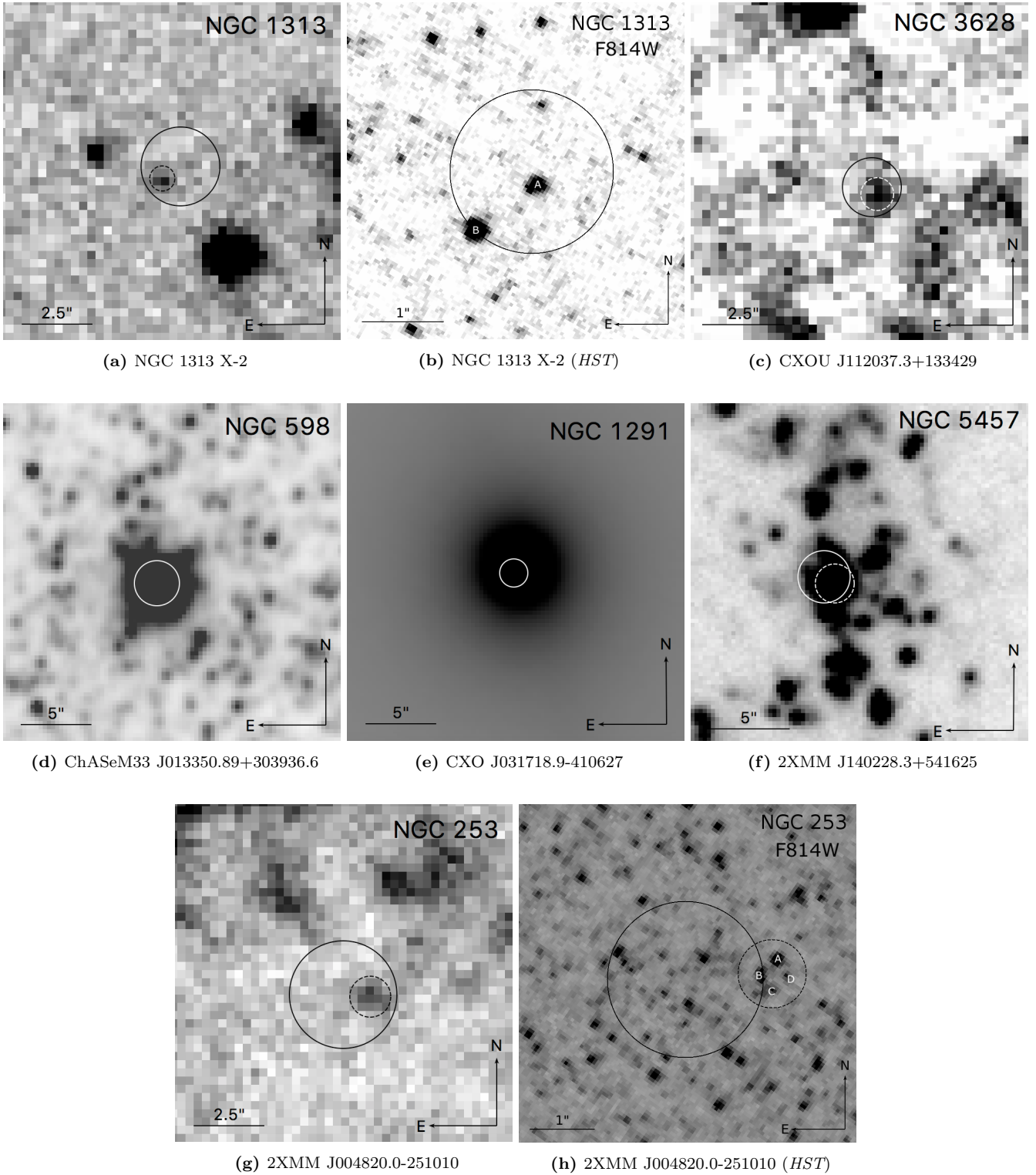


Figure 1. Finder charts of the ULXs with a NIR candidate counterpart. The black/white solid circles correspond to the 99.7% confidence region of the position of the ULXs, whereas the black/white dashed circles mark the candidate counterpart as detected with SExtractor. Images are in the *H*-band, unless indicated otherwise.

magnitudes consistent with being a faint RSG, whereas the source we labeled as A is bluer and consistent with it being an O-B type star, as previously reported. On our H -band image, we only detect one candidate counterpart within the 99.7% confidence radius (see Figure 1a). It has an absolute magnitude of $H = -7.1 \pm 0.2$, i.e. this source is also consistent with being a faint RSG. Alternatively, (part of) the NIR emission could be due to nebular emission lines. NGC 1313 X-2 is surrounded by a bright optical nebula (e.g. Pakull & Grisé 2008) and these ULX nebula often show strong emission lines in the NIR (e.g. Heida et al. 2016; López et al. 2019, this work, see Section 5.4). In conclusion, neither source A nor source B have definite characteristics that prove whether one of them is the donor star to the ULX.

5.1.2 CXOU J112037.3+133429

This ULX in NGC 3628 was observed by Heida et al. (2014) in the K_s -band, where they did not detect a counterpart, to a limiting magnitude of -11.2 . We re-observe it in the H -band and detect one candidate counterpart within its 99.7% confidence radius (see Figure 1c). The detected source has an absolute magnitude of $H = -9.7 \pm 0.5$, consistent with the absolute magnitude of a RSG. We can estimate a $H - K_s$ color from these two observations, although we must note that they were performed 5.5 years apart. The counterpart would have $H - K_s < 1.5 \pm 0.5$ which is consistent within uncertainties with the values for a typical RSG (Elias et al. 1985; Drilling & Landolt 2000).

5.2 Possible NIR star cluster candidates

As we give this classification to any source whose absolute magnitude is too bright to be a RSG and unlikely to be an AGN as it is spatially extended, it is a preliminary, rough categorization. Considering that the only SC candidate that we have spectroscopically followed-up turned out to be a nebula (see Section 5.4.4), we cannot ignore that there is a possibility that the sources below might as well also be nebulae.

5.2.1 ChASem33 J013350.89+303936.6

This source was detected in NGC 598 in early X-ray observations (e.g. Long et al. 1981; Markert & Rallis 1983). Its *Chandra* X-ray position coincides with the nucleus of NGC 598 (Dubus & Rutledge 2002). No sign of nuclear activity at other wavelengths was detected (Dubus et al. 2004), thus it was classified as a ULX. We detect one NIR candidate counterpart (see Figure 1d) within the 99.7% confidence radius, with absolute magnitude of $H = -13.0 \pm 0.1$ mag. However, this source location is consistent with that of the nucleus of NGC 598 and thus, the NIR emission is dominated by the nucleus of the galaxy. We cannot resolve the counterpart, and moreover, it is likely that we are detecting a nuclear star cluster.

5.2.2 CXO J031718.9-410627

This potential ULX in NGC 1291 has one NIR candidate counterpart (see Figure 1e) and, similarly to the case of the

ULX in NGC 598, its position is consistent with that of the nucleus of the galaxy. Hence, we cannot distinguish if the emission comes from an individual source or if its contaminated/dominated by the nucleus of NGC 1291. We deem it likely that we are detecting a nuclear star cluster.

5.2.3 2XMM J140228.3+541625

This ULX has one NIR candidate counterpart (see Figure 1f) with an absolute magnitude of $H = -13.2 \pm 0.1$, too bright to be a single star. The FWHM of this extended source is $0.9''$ which is set by the seeing. At the distance of NGC 5457 this is equivalent to 30 pc. The size is therefore smaller than 30 pc, but we cannot rule out that it is a stellar cluster (see Merritt et al. 2009).

5.3 NIR candidate without classification

5.3.1 2XMM J004820.0-251010

For this ULX in NGC 253, we detect a counterpart inside the 99.7% confidence radius of its X-ray position, (see Figure 1g) with an absolute magnitude of $H = -7.4 \pm 0.2$, consistent with the faint end of a RSG. However, when we analyse archival *HST* images of this source in the F606W and F814W filters (observation ID 10915), taken from the Barbara A. Mikulski Archive for Space Telescopes (MAST)³, we find something different. At the position of our NIR counterpart detection (the dashed circle in Figures 1g and 1h), the *HST* images allow us to resolve it into at least four point-like sources. SExtractor detected only four sources, for which we calculate apparent and absolute R and I band Vega magnitudes (see Table 6). These sources are all too faint for a RSG, even after we consider possible extinction in both bands (see Table 6). There are also other point-like sources inside the 99.7% confidence radius of the X-ray position which we do not detect in our H -band image. Therefore, none of these sources has a color red enough for it to be a RSG, and we conclude that the source we detected in the NIR observation is in fact a blend of the resolved source detected in the HST image.

5.4 Spectroscopy

5.4.1 RX J073655.7+653542: a RSG in NGC 2403

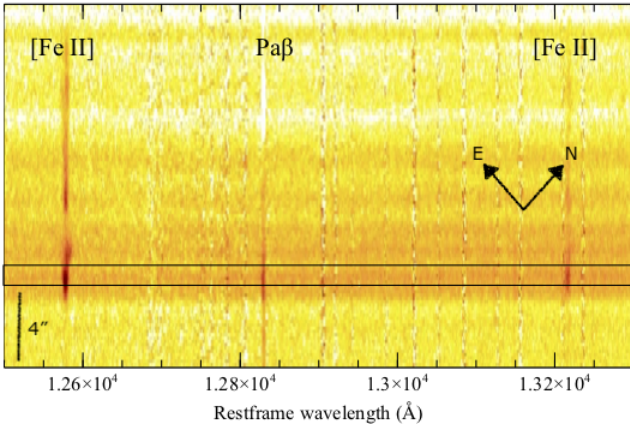
This X-ray source is located inside a large extended nebula. Our 2-D J -band spectrum reveals strong [Fe II] $\lambda 1257$ emission around the ULX with an extent of $\sim 3''$, as well as emission extending up to $\sim 12''$ along the slit offset from the position of the ULX (see Figure 2a). At the distance to NGC 2403, these values correspond to physical sizes of ~ 35 and ~ 240 pc. This same structure is not visible in the $\text{Pa}\beta$ line, possibly due to strong emission in that line on the other side of the ULX that shows up in absorption at the location of the extended [Fe II] emission due to our nodding pattern. The [Fe II] $\lambda 1257$ line is redshifted by 175 ± 5 km s^{-1} , consistent with the radial motion of NGC 2403. In

³ <https://mast.stsci.edu/portal/Mashup/Clients/Mast/Portal.html>

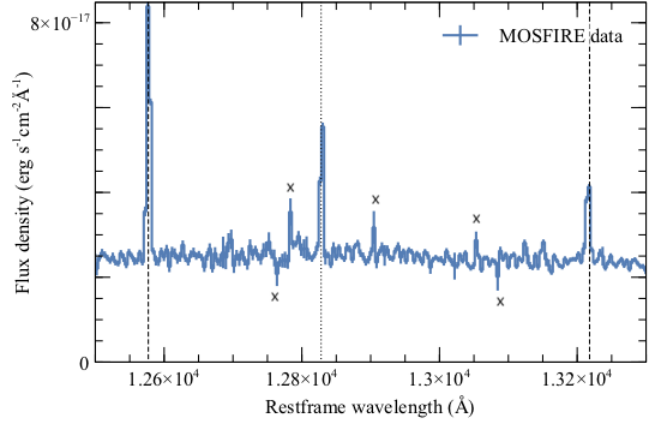
Table 6. Counterparts detected in archival *HST* images for four of our observed ULXs. We provide their apparent and absolute Vega magnitudes, and their respective intrinsic colours. The labels A, B, C and D are the same as used in Figures 1b and 1h to mark the counterparts.

ULX name	Apparent magnitude (mag)		Absolute magnitude (mag)		Extinction* (mag)	Colour (mag)
NGC 1313 X-2	$V_A = 23.58 \pm 0.33$	$V_B = 24.66 \pm 0.55$	$V_A = -4.88 \pm 0.37$	$V_B = -3.80 \pm 0.58$	$A_V = 0.32$	$(V - I)_A = 0.13 \pm 0.69$
	$I_A = 23.56 \pm 0.56$	$I_B = 22.84 \pm 0.40$	$I_A = -4.76 \pm 0.59$	$I_B = -5.48 \pm 0.44$	$A_I = 0.18$	$(V - I)_B = 1.68 \pm 0.72$
	$J_A = 24.01 \pm 0.41$	$J_B = 22.38 \pm 0.19$	$J_A = -4.28 \pm 0.48$	$J_B = -5.91 \pm 0.31$	$A_J = 0.08$	
2XMM J004820.0-251010	$R_A = 25.59 \pm 0.43$	$I_A = 23.74 \pm 0.34$	$R_A = -2.27 \pm 0.46$	$I_A = -4.09 \pm 0.38$	$A_R = 0.10$	$(R - I)_A = 1.83 \pm 0.60$
	$R_B = 27.22 \pm 0.95$	$I_B = 25.71 \pm 0.85$	$R_B = -0.64 \pm 0.97$	$I_B = -2.12 \pm 0.87$	$A_I = 0.08$	$(R - I)_B = 1.49 \pm 1.30$
	$R_C = 26.00 \pm 0.55$	$I_C = 24.68 \pm 0.53$	$R_C = -1.85 \pm 0.58$	$I_C = -3.16 \pm 0.56$		$(R - I)_C = 1.30 \pm 0.80$
	$R_D = 26.64 \pm 0.74$	$I_D = 25.28 \pm 0.69$	$R_D = -1.22 \pm 0.76$	$I_D = -2.56 \pm 0.71$		$(R - I)_D = 1.34 \pm 1.04$
RX J073655.7+653542	$J_A = 20.56 \pm 0.12$	$H_A = 19.68 \pm 0.15$	$J_A = -7.10 \pm 0.22$	$H_A = -7.90 \pm 0.24$	$A_H = 0.06$	$(J - H)_A = 0.72 \pm 0.32$
	$J_B = 20.49 \pm 0.12$	$H_B = 19.50 \pm 0.12$	$J_B = -7.17 \pm 0.22$	$H_B = -8.07 \pm 0.22$	$A_J = 0.15$	$(J - H)_B = 0.96 \pm 0.31$
CXOU J140314.3+541807	$V_A = 24.76 \pm 0.53$	$I_A = 22.39 \pm 0.18$	$V_A = -4.90 \pm 0.56$	$I_A = -7.07 \pm 0.26$	$A_V = 0.25$	$(V - I)_A = 2.17 \pm 0.62$
	$V_B = 24.84 \pm 0.54$	$I_B = 23.82 \pm 0.36$	$V_B = -4.82 \pm 0.57$	$I_B = -5.64 \pm 0.40$	$A_I = 0.46$	$(V - I)_B = 0.82 \pm 0.69$
	$V_C = 23.13 \pm 0.23$	$I_C = 23.06 \pm 0.25$	$V_C = -6.54 \pm 0.28$	$I_C = -6.40 \pm 0.31$		$(V - I)_C = -0.14 \pm 0.43$
	$V_D = 23.11 \pm 0.23$	$I_D = 22.86 \pm 0.23$	$V_D = -6.55 \pm 0.30$	$I_D = -6.60 \pm 0.29$		$(V - I)_D = 0.05 \pm 0.42$

Notes: *Calculated using $N_H = 6.04 \times 10^{20}$ atoms cm^{-2} for NGC 1313 X-2, $N_H = 2.55 \times 10^{20}$ atoms cm^{-2} for 2XMM J004820.0-251010, $N_H = 1.19 \times 10^{21}$ atoms cm^{-2} for RX J073655.7+653542 and $N_H = 8.52 \times 10^{20}$ atoms cm^{-2} for CXOU J140314.3+541807 (values taken from HI4PI Collaboration et al. 2016).



(a) RX J073655.7+653542



(b) RX J073655.7+653542

Figure 2. (a) Part of the 2-D *J*-band spectrum of RX J073655.7+653542, centered on the two [Fe II] emission lines. The horizontal black lines indicate the location of the continuum source at the X-ray position of the ULX. The [Fe II] emission extends for $\sim 3''$ around the ULX, with a larger region extending out to $\sim 12''$ towards the north-east. (b) MOSFIRE *J*-band spectrum of RX J073655.7+653542 (blue, with errorbars). The [Fe II] emission lines are indicated by dashed lines, the dotted line shows the position of the strongest Paschen line in the band. All wavelengths are in vacuum.

addition, there is a continuum source at the location of the ULX that is very likely stellar in origin (see Figure 2b).

Three Fe I absorption lines are visible in the 1.15–1.17 μm region of the spectrum (see Figure 4a). We cross-correlated our spectrum with PHOENIX model atmospheres for RSGs with temperatures of 3000, 4000 and 5000 K and $\log(g) = -0.5$ (Lançon et al. 2007) in the 1.15–1.17 μm region. From the three model atmospheres that we tested, the 4000 K model best matches our spectrum; the 3000 K model contains a strong CO bandhead at 1.24 μm that is not present in our data, while the slope of the 5000 K model is too blue. The 4000 K model moreover yields the strongest cross-correlation signal. The RVs found through

cross-correlating the three different templates are all consistent. We therefore conclude that this star most likely has an effective temperature in the 3500 – 4500 K range. For the RV, we adopt the value found through cross-correlating with the 4000 K model: 160 ± 12 km s^{-1} . This is consistent (within $2\text{-}\sigma$) with the RV of the emission lines and with the radial velocity of NGC 2403 at the position of the ULX (~ 170 km s^{-1} , Fraternali et al. 2002).

We further examine these results by analysing the archival *HST* images of this source in the F110W and F160W filters. At the position of the ULX, we detect two bright sources, the one labeled as B is at the position reported by López et al. (2017) (see Figure 3a). Their apparent, abso-

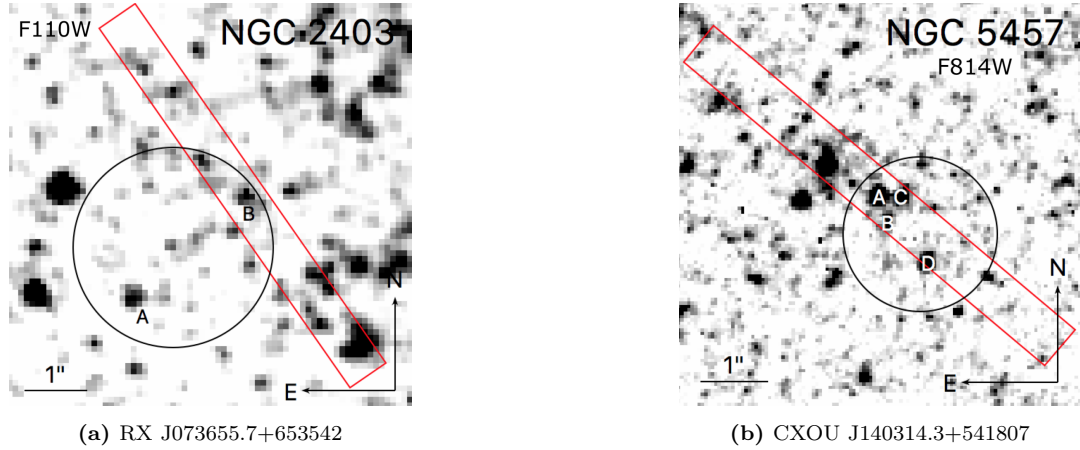


Figure 3. *HST* finder charts for the ULXs (a) RX J073655.7+653542 and (b) CXOU J140314.3+541807. The solid circles correspond to the 99.7% confidence region of the position of the ULXs, the letters mark the sources detected with SEXTRACTOR, and the $0.7''$ -MOSFIRE-slit-width is indicated in red. For presentation purposes, the slit length is set to $7''$; however, a $0.7'' \times 110.7''$ slit was used for (a) and a $0.7'' \times 118.7''$ slit was used for (b).

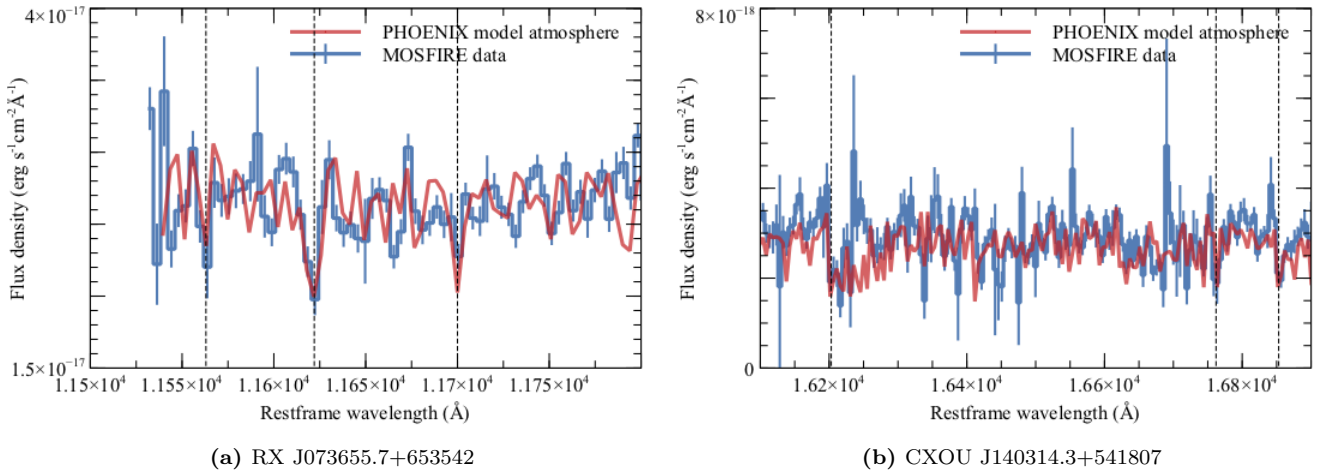


Figure 4. (a) Part of the MOSFIRE *J*-band spectrum of RX J073655.7+653542 (blue, with errorbars) is shown along with the 4000 K PHOENIX model atmosphere (red), redshifted by 160 km s^{-1} to match the radial velocity of the star. Dashed lines indicate the positions of strong Fe I absorption features. (b) Part of the MOSFIRE *H*-band spectrum of CXOU J140314.3+541807 (blue, with errorbars) is shown along with the 3000 K PHOENIX model atmosphere (red), redshifted by 190 km s^{-1} to match the radial velocity of the star. Dashed lines indicate the positions of some strong absorption features found in RSGs. All wavelengths are in vacuum.

lute Vega magnitudes and extinction are indicated in Table 6 and from them, we can see that the source we labeled B has absolute magnitudes consistent with being a RSG, if in the faint end. However, we can see in the image that there are several other unresolved sources, which opens the possibility of both sources A and B being contaminated by the light of these groups of stars. This could result in fainter *J*- and *H*-band magnitudes, weakening the claim that RX J073655.7+653542 is a RSG. An adaptive optics assisted spectrum, reducing as much as possible the potential contamination of the spectrum by light from currently unresolved nearby stars, will provide important new information on the nature of the candidate counterpart to ULX RX J073655.7+653542.

5.4.2 CXOU J140314.3+541807: a RSG in NGC 5457

Our *H*-band spectrum of this source shows a continuum with absorption features, most notably several CO-bandheads. We cross-correlate this spectrum with PHOENIX model atmospheres with effective temperatures of 3000, 4000 and 5000 K, using the spectral range from $1.615\text{--}1.69 \mu\text{m}$, where several strong absorption features are seen (see Figure 4b). The cross-correlation with the 3000 K model yields the strongest signal; the cross-correlation with the 4000 K model gives a consistent result but weaker signal, and the cross-correlation with the 5000 K model does not show significant peaks. We adopt the radial velocity obtained from the cross-correlation with the 3000 K model, of $193 \pm 17 \text{ km s}^{-1}$. This is consistent with the radial velocity of NGC 5457 at the position of the ULX (i.e. $\sim 200 \text{ km s}^{-1}$ Hu et al. 2018). We

conclude that this source is most likely a red supergiant with an effective temperature in the 3000 – 4000 K range, matching the classification based on mid-IR photometry presented in Lau et al. (2019).

We also examine these results by analysing the archival *HST* images of this source in the F555W and F814W filters. At the position of the ULX, we detect four bright sources, one of them (A) at the position reported by Heida et al. (2014) (see Figure 3b). Their apparent, absolute Vega magnitudes and extinction are indicated in Table 6 and from them, we can see that the source labeled A has absolute magnitudes consistent with being a RSG. However, we can see in the image that inside the $3\text{-}\sigma$ confidence position radius, there are three bright bluer sources. There is no physical reason that rules out these sources as possible donor stars to the ULX. A second epoch spectrum from our NIR counterpart would confirm its association with the ULX, if radial velocity variations are detected.

5.4.3 XMMU J024323.5+372038: a likely AGN

The spectrum of this counterpart in NGC 1058 is dominated by a broad emission line, reminiscent of the broad $H\alpha$ emission profile often seen in AGNs (see e.g. Coatman et al. (2016)). Hence, we deem it reasonable to fit Gaussian profiles to the structure, fixing the relative spacing between $H\alpha$ and [NII] a line ratio of 1:3 for the [NII] λ 6549:[N II] λ 6583 lines (Osterbrock 1989), with redshift, amplitude and FWHM as free parameters. As a result, we see a broad component and the three narrow lines: $H\alpha$ and [N II] λ 6548, 6583 (see Figure 5a). This would yield a redshift of $z = 1.0301 \pm 0.0001$, making XMMU J024323.5 + 372038 a likely background AGN.

5.4.4 [LB2005] NGC 5457 X26: a nebula

This source was preliminarily classified as a stellar cluster by López et al. (2017) based on its absolute magnitude (-11.44 ± 0.22) and spatial extent. Its H -band spectrum is dominated by a strong [Fe II] emission line. Several other [Fe II] weaker lines and two Bracket lines are detected as well (see Figure 5b). After fitting Gaussian profiles to these lines, we calculated the radial velocity of the source to be $295 \pm 16 \text{ km s}^{-1}$, consistent with the radial velocity of NGC 5457 at the position of the ULX (Hu et al. 2018).

5.4.5 2E 1402.4+5440: an unknown source

This source in NGC 5457 has an apparent and absolute H -band magnitude of 19.3 ± 0.2 and -9.9 ± 0.2 , respectively. Its spectrum shows a weak continuum (see Figure 6a) and some emission lines appear to be present. However, these apparent emission lines are residuals from the subtraction of the sky emission as they lie close to strong strong emission lines (see Figure 6b). No clear absorption or emission lines are detected. Therefore, we conclude that this source does not host a strong nebula, but the continuum emission could be coming from an accretion disk or a RSG (or a combination of the two).

6 RECAPITULATION OF OUR NIR IMAGING SURVEY

6.1 Host galaxies to observed ULXs

In the span of 8 years we have studied 113 ULXs in 52 different galaxies, up to a distance of $\simeq 10$ Mpc (see Figure A1a), within uncertainties. These 113 ULXs were located at a distance range of 0.5 pc to 29 kpc from the centre of their respective host galaxies (see Figure A1b).

Of the 52 galaxies, we observed two or more ULXs in 21 galaxies and only one ULX in each of the remaining 31 galaxies. We made use of 5 different telescopes and the H , K_s photometric bands. We tailored the survey to detect RSGs by aiming to achieve a depth of 20 mag in H and K_s . Considering that the distances to the observed sources range from 0.91 ± 0.5 to 14.19 ± 2.84 Mpc, our expected depth was $-10.8 \pm 0.4 < H, K_s < -4.8 \pm 0.1$ mag.

We could not observe all ULXs located within 10 Mpc, as the total number of ULX within 10 Mpc is 170. This was due to several factors such as not being able to use the telescope due to adverse weather conditions.

6.2 Detected NIR counterparts

Out of the 113 observed ULXs, we detected a NIR candidate counterpart for 38 ULXs, i.e. about a third of the total sample. Based only on photometry, of the 38 detected NIR counterparts, 20 have NIR colours and/or magnitudes consistent with a RSG, 11 are preliminarily classified as stellar clusters, six are consistent with being an AGN and one is too faint to be either a RSG or a SC/AGN (see Table B1). After spectroscopic follow-up of 12 out of these 38 counterparts, we confirmed five RSGs (Heida et al. 2015a, 2016 and this work), while four sources photometrically classified as RSG turned out to be nebulae (Heida et al. 2016; López et al. 2019 and this work). For the remaining 3 followed-up sources, one RSG candidate is a background AGN (this work), one stellar cluster candidate turned out to be a nebula (this work, see Table B1) and the last RSG candidate is too faint to be classified. This means that currently we have 5 confirmed RSGs and ten RSG candidates (photometrically classified).

The distribution of the detected counterparts in terms of their distance to our Galaxy (see Figure A1a) most likely follows the distribution of observed ULXs, based on the Kolmogorov–Smirnov (K–S) test between them (p-value = 0.88). For the distribution of detected counterparts in terms of their distance to the centre of their host galaxies (see Figure A1b), we find that it also most likely follows the distribution of observed ULXs, with a p-value = 0.67. In addition, we detect a counterpart to all observed ULXs located at > 15 kpc from their host galaxy centre, which could be due to the ULXs having no contamination from their host galaxy, making the detection of a counterpart easier.

The detected counterparts in the H -band have an apparent magnitude ranging from 12 to 22 and an absolute magnitude from -18 to -7 , those detected in the K_s -band have an apparent magnitude ranging from 15 to 22 mag and an absolute magnitude from -15 to -8 (see Figure A2). We compare the distribution of our 15 detected RSGs (five confirmed and 10 photometrically classified) with the K_s absolute magnitudes distribution of 85 RSGs in the Milky Way

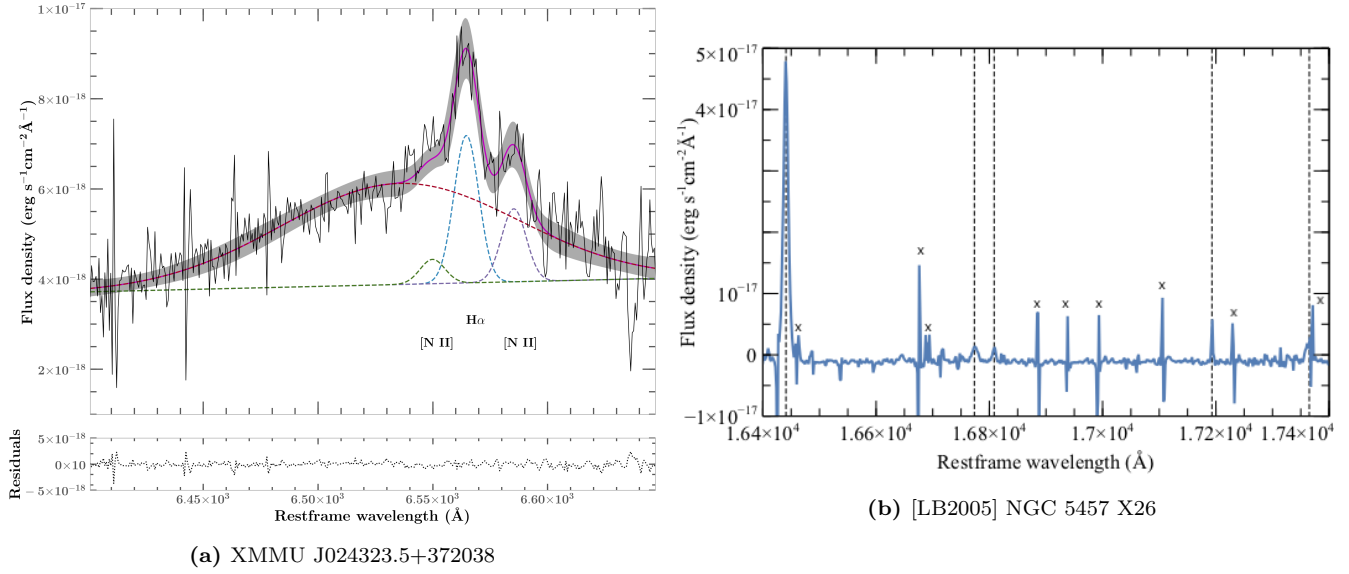


Figure 5. (a) Part of the NIR spectrum of XMMU J024323.5 + 372038 showing the broad and narrow components of the emission line. The Gaussian profiles are shown indicating the position of the putative [N II] $\lambda\lambda$ 6548, 6583 and H α lines. The shaded area shows the 3- σ confidence region around the fit. The residuals of the fit are shown in the bottom panel. (b) Part of the NIR spectrum of [LB2005] NGC 5457 X26 where the dashed lines indicate the positions of the nebular [Fe II] and Brackett emission lines, redshifted by 295 km s $^{-1}$. Residuals of sky lines subtraction or spurious lines are marked with an x. All wavelengths are in vacuum.

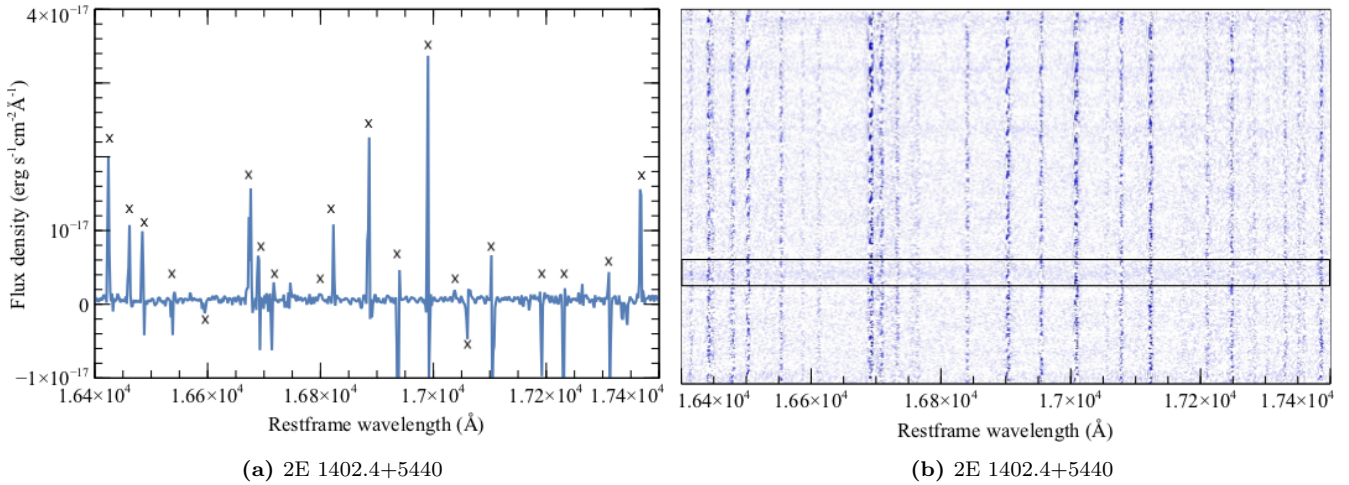


Figure 6. (a) Part of the NIR spectrum of 2E 1402.4 + 5440. (b) Part of the 2-D spectrum of 2E 1402.4 + 5440 showing the same wavelength range as in (a). The faint continuum is inside the solid rectangle. Residuals of sky lines subtraction or spurious lines are marked with an x. All wavelengths are in vacuum.

(MW) and the Large Magellanic Cloud (LMC) (Levesque et al. 2005), and with the K_s absolute magnitudes distribution of 245 RSGs in the Andromeda galaxy (M31) (Massey & Evans 2016). A K-S test between these two distributions show that they are not similar (p-value = 6.6×10^{-9}). We also compare our RSGs distribution with all 330 RSGs in the MW, LMC and M31 (see Figure A2b). We assume a colour of $H - K_s \simeq 0$, typical for RSGs (Elias et al. 1985; Drilling & Landolt 2000). A K-S test between ours and the distribution of RSGs in the MW and the LMC shows that our detected RSGs are most likely drawn from the distribution

of RSGs in the MW/LMC (p-value = 0.54). We reach the same conclusion when comparing our RSG distribution with that of M31 (p-value = 0.08) and that of MW/LMC/M31 (p-value = 0.38).

6.3 Probability of chance superposition

More than 50% and 80% of the observed ULXs are located at less than 5 and 10 kpc, respectively, from the nucleus of their host galaxies (see Figure A1a). This could result in ULXs being in crowded environments (i.e. close to the nucleus, in

Table 7. The 38 identified NIR candidate counterparts to ULXs. The preliminary classification of the NIR candidate counterparts is based on their absolute magnitudes, WISE colours, spatial extent and/or visual inspection of the NIR image. The spectroscopic classification of 12 sources is based on the spectra that we obtained for them, reported in Heida et al. (2015a, 2016) and López et al. (2019).

Galaxy	ULX name (in SIMBAD)	Filter	Apparent magnitude (mag)	Absolute magnitude (mag)	Preliminary classification	Spectroscopic classification
NGC 253	RX J004722.4 – 252051	K_s	17.2 ± 0.5	-10.5 ± 0.1	RSG	RSG
NGC 253	2XMM J004820.0 – 251010	H	20.4 ± 0.1	-7.4 ± 0.2	N/A	–
NGC 598	ChASeM33 J013350.89 + 303936.6	H	11.8 ± 0.1	-13.0 ± 0.1	SC	–
NGC 925	[SST2011] J022721.52 + 333500.7	H	18.7 ± 0.2	-10.6 ± 0.4	RSG	RSG
NGC 925	[SST2011] J022727.53 + 333443.0	H	20.1 ± 0.2	-9.2 ± 0.4	RSG	Nebula
NGC 1058	XMMU J024323.5 + 372038	H	20.8 ± 0.3	-9.0 ± 0.4	RSG	AGN
NGC 1291	CXO J031718.9 – 410627	H	11.3 ± 0.1	-18.4 ± 0.1	SC	–
NGC 1313	NGC 1313 X-2	H	21.1 ± 0.2	-7.1 ± 0.2	RSG	–
NGC 1637	[IWL2003 68]	K_s	16.3 ± 0.5	-13.7 ± 0.5	SC/AGN	–
NGC 2403	RX J073655.7 + 653542	H	17.46 ± 0.02	-10.1 ± 0.2	RSG	RSG
NGC 2500	CXO J080157.8 + 504339	K_s	15.7 ± 0.2	-14.1 ± 0.4	AGN	–
Holmberg I	[WMR2006] Ho I XMM1	H	17.1 ± 0.1	-10.14 ± 0.1	AGN	–
Holmberg II	Holmberg II X-1	H	20.6 ± 0.1	-7.1 ± 0.1	RSG	Nebula
NGC 3521	[SST2011] J110545.62 + 000016.2	H	19.8 ± 0.1	-10.9 ± 0.9	RSG	Nebula
NGC 3627	[SST2011] J112018.32 + 125900.8	K_s	20.6 ± 1.9	-9.1 ± 1.9	RSG	–
NGC 3628	CXOU J112037.3 + 133429	H	20.4 ± 0.2	-9.7 ± 0.5	RSG	–
NGC 4136	CXOU J120922.6 + 295551	H	19.1 ± 0.1	-10.78 ± 0.4	RSG	Nebula
NGC 4136	[SST2011] J120922.18 + 295559.7	H	19.2 ± 0.1	-10.75 ± 0.4	RSG	RSG
NGC 4258	RX J121844.0 + 471730	H	17.8 ± 0.1	-11.5 ± 0.1	SC	–
NGC 4258	3XMM J121847.6 + 472054	H	20.1 ± 0.1	-9.3 ± 0.2	RSG	–
NGC 4258	[LB2005] NGC 4258 X9	H	15.86 ± 0.001	-13.5 ± 0.2	AGN	–
NGC 4485	RX J1230.5 + 4141	H	19.0 ± 0.1	-10.7 ± 0.4	RSG	–
NGC 4490	[SST2011] J123029.55 + 413927.6	H	16.05 ± 0.01	-13.4 ± 0.3	SC	–
NGC 4490	CXO J123038.4 + 413831	H	16.69 ± 0.01	-12.8 ± 0.3	RSG	–
NGC 4490	2XMM J123043.1 + 413819	H	18.41 ± 0.04	-11.0 ± 0.3	SC	–
NGC 4559	[SST2011] J123557.79 + 275807.4	H	17.33 ± 0.01	-11.99 ± 0.90	SC	–
NGC 4559	RX J123558 + 27577	H	18.95 ± 0.05	-10.4 ± 0.9	RSG	–
NGC 4594	[LB2005] NGC 4594 X5	H	18.65 ± 0.02	-11.6 ± 0.6	AGN	–
NGC 4631	[SST2011] J124211.13 + 323235.9	H	14.48 ± 0.001	-14.85 ± 0.49	SC	–
NGC 5194	XMMU J132953.3 + 471040	H	15.7 ± 0.1	-13.88 ± 0.2	SC	–
NGC 5194	RX J132947 + 47096	H	18.60 ± 0.04	-11.18 ± 0.04	RSG	–
NGC 5408	NGC 5408 X-1	K_s	20.3 ± 0.2	-8.1 ± 0.8	RSG	–
NGC 5457	2E 1402.4 + 5440	H	19.3 ± 0.2	-9.7 ± 0.2	RSG	N/A
NGC 5457	2XMM J140248.0 + 541350	H	17.7 ± 0.1	-11.3 ± 0.1	RSG	RSG
NGC 5457	CXOU J140314.3 + 541807	H	18.4 ± 0.1	-10.7 ± 0.1	AGN	–
NGC 5457	[LB2005] NGC 5457 X32	H	18.67 ± 0.02	-10.5 ± 0.1	AGN	–
NGC 5457	[LB2005] NGC 5457 X26	H	17.78 ± 0.01	-11.4 ± 0.2	SC	Nebula
NGC 5457	2XMM J140228.3 + 541625	H	16.0 ± 0.1	-13.2 ± 0.1	SC	–

spiral arms of the galaxy, etc), so the probability of a chance superposition of an unrelated object may not be negligible. Using SExtractor, we search for point sources with an absolute magnitude in the RSG range ($-11 < H, K_s < -8$) in all the images of our 113 ULXs. We then measure the total area of each image in arcsec² and the area of the error circle around the X-ray position of each ULX (also in arcsec²).

These values, along with the detected point sources, allow us to estimate the probability of finding a source with an absolute magnitude in the RSG range for each of the 113 ULXs. See the probability distribution in Figure 7. More than 90 out of the 113 observed ULXs have $\leq 5\%$ chance superposition probability, whereas six ULXs have a proba-

bility between 20–30%. For only one of these six ULXs a candidate RSG counterpart was detected (NGC 5408 X-1, Heida et al. 2014).

We calculate the total probability of a chance superposition for the sample of 113 ULXs as 3.3%, which means that we could have 3.7 positives in our detections. We note that the distribution of stars in a galaxy is inhomogeneous, and the value of a chance superposition depends on the part of the image selected for the observation, for which we cannot calculate an accurate value for this probability, only provide a rough estimate. Based on this, we could expect that up to four of our 38 counterparts may be chance superpositions.

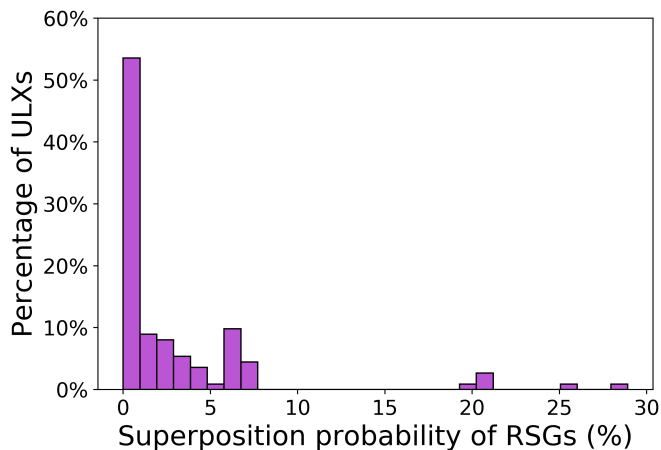


Figure 7. Histogram of the distribution of probabilities of a chance superposition of a source with an absolute magnitude in the RSG range for all 113 observed ULXs. The bins have a 1% probability width, for visualization purposes.

6.4 Non-detections

For the 75 ULXs for which we did not detect a candidate counterpart, we calculated the limiting magnitude at the position of the ULX. In the H -band, the limiting apparent (absolute) magnitude ranges from 16 to 22 (-13 to -6), whereas in the K_s band, the limiting apparent (absolute) magnitude ranges from 18 to 22 (-12 to -7). The distribution of these values can be seen in Figure A3.

Examining Figure A3 we can see that at the position of 67 out of these 75 ULXs, we reached the depth necessary to be able to detect the bright end of the distribution of the absolute magnitude of RSGs, i.e. $H, K_s > -11$ mag. Of these 67 sources, for seven ULXs the limiting absolute magnitude at their position is fainter than the faintest absolute magnitude for a RSG ($H, K_s > -8$). We can draw one conclusion for these seven ULXs: the donor star is certainly not a RSG (see e.g. Levesque et al. 2005; Kiss et al. 2006; Massey & Evans 2016). This means that for 60 ULXs, the limiting absolute magnitude at their position is within the range of a typical RSG, i.e. $-11 < H, K_s < -8$. Of these 60 ULX, for 18 ULXs we probe the brightest end for a RSG ($-11 < H, K_s < -10$, M3 spectral type or later). For 28 ULXs we probe the intermediate RSG range ($-10 < H, K_s < -9$, K5 spectral type or later); and for 14 ULXs, we probe the faint end ($-9 < H, K_s < -8$, K0 spectral type or later).

We compare this distribution to the K_s absolute magnitudes distribution of the 330 RSGs in the MW, the LMC, and M31. As can be seen from Figure A2b, about 12% of these have absolute magnitudes brighter than -11 mag; almost one-third of the RSGs are in the brightest end for a RSG, i.e. $-11 < H, K_s < -10$; $\simeq 40\%$ of the RSGs are between -10 and -9 mag and about 15% are in the faint end ($-9 < H, K_s < -8$). In light of this, we can only rule out the presence of a bright RSG ($-11 < H, K_s < -10$) for the 42 ULXs for which the limiting magnitude is $-10 < H, K_s < -8$. For the remaining eight ULXs out of the 75 with non-detections, our limiting absolute magnitude at the position of the ULX is $H, K_s < -11$ mag, due to crowding or high background from the host galaxies. This prevents

us from actually concluding if there is a RSG counterpart (or not) to these eight ULXs, as only 12% of RSGs are that bright.

6.5 Spectroscopically observed NIR counterparts

At the time of writing this manuscript, only seven counterparts had been spectroscopically followed-up by Heida et al. (2015a), Heida et al. (2016) and López et al. (2019). All seven sources have an absolute magnitude consistent with being RSGs. Heida et al. (2015a) confirmed the nature of a RSG in the galaxy NGC 253. Heida et al. (2016) observed 5 sources and confirmed the nature of two more RSGs, in the galaxies NGC 925 and NGC 4136. Three sources turned out to be nebulae (in NGC 925, in Holmberg II and NGC 4136). López et al. (2019) followed-up a candidate RSG in NGC 3521 identified by López et al. (2017). Its spectral signatures single this source out as a nebula. In this manuscript, we analyse the nature of five more sources out of those 38 counterparts: four candidate RSGs and one candidate stellar cluster (see Table B1). Of the four candidate RSGs, one cannot be classified, the other one is most likely a background AGN and the other two sources show absorption lines consistent with them being RSGs. Additionally, we show that a source originally classified as a stellar cluster by López et al. (2017) is actually a nebula (see Section 5b).

In summary, we have confirmed the RSG nature for five sources. We need to additionally corroborate if these confirmed RSGs are the actual donor stars of the ULXs by detecting radial velocity variations. If we corroborate this for our five confirmed RSGs, this would imply that $\simeq (4 \pm 2)\%$ of the observed ULXs have a RSG donor star, about four times more than predicted by binary evolution models (see e.g. Wiktorowicz et al. 2017).

Of our 11 followed-up candidate RSGs, $(36 \pm 18)\%$ are actually nebulae and $(45 \pm 20)\%$ are in fact RSGs, which potentially implies that of our remaining ten RSG candidate counterparts, half could be confirmed as RSG and the other half as nebulae (i.e., we cannot distinguish a RSG from a nebulae based only on our broadband photometry). If these numbers hold, it means that we will have ten confirmed RSGs for a sample of 113 observed ULXs. If we further corroborate their donor star nature, this would mean that $\simeq (10 \pm 3)\%$ of the ULXs would have a RSG donor star, a number 10 times larger than predicted by Wiktorowicz et al. (2017).

7 CONCLUSIONS

This is the third and last paper on the systematic photometric search for NIR counterparts to ULXs. We observed 23 ULXs in 15 galaxies and detected a candidate counterpart for six of them. For the ULXs with non-detections, we report limiting apparent and absolute magnitudes. Two ULXs have candidate counterparts with absolute magnitudes consistent with a RSG. Three candidates are too bright to be single RSGs, and after visual inspection of their NIR images and/or determination of their size, we conclude that they are more likely to be star clusters. The remaining candidate counterpart is too faint to either be a RSG or a star cluster. We also spectroscopically followed-up four RSG candidates

identified by Heida et al. (2014) and a stellar cluster candidate identified by López et al. (2017). The stellar cluster candidate turned out to be a nebula, showing strong [Fe II] emission. As for the RSG candidates, one source cannot be classified as significant absorption or emission lines were not detected, and another one has a spectrum dominated by a broad putative H α emission line, making it likely a background AGN at $z = 1.0301 \pm 0.0001$. However, the other two sources show stellar spectra consistent with them being RSGs.

Evaluating the complete search presented in Heida et al. (2014) and López et al. (2017) and this work, we found that we have observed 113 ULXs in 52 different galaxies using 5 different telescopes and the H, K_s -bands. The ULXs are located at a distance range 0.5 to 29 kpc from the centre of their respective host galaxies. These galaxies are up to a distance of $\simeq 10$ Mpc. We detected a NIR candidate counterpart for 38 ULXs out of the 113 ULXs, i.e. roughly one-third of the total sample. In addition to these detections, we reached our expected depth, i.e. $H, K_s < -11$ at the position of 67 ULXs, although we did not detect a counterpart. Of the 38 detected counterparts, we have 27 sources preliminarily classified based only on broadband photometry. Ten of these candidate counterparts are candidate RSGs, 10 are candidate stellar clusters, six are candidate AGN and one is too faint to be either a RSG or a SC/AGN. We estimate the probability of a chance superposition for the whole sample of 113 ULXs as 3.3%, which means that up to four of our detections could be false positives.

We have confirmed the nature of 11 sources by spectroscopic observations. For these, we have five RSGs, one AGN and five nebulae. As four of the five nebulae were originally classified as RSGs, it shows that RSGs and nebulae are difficult to distinguish in terms of broadband photometry. Moreover, if we can determine that our five spectroscopically confirmed RSGs are in fact the donor stars of the ULXs, via detection of radial variations, these possible ULX-RSG binary systems are in contrast with the predictions from the binary evolution simulations from Wiktorowicz et al. (2017). Our results could be at least four times (and maybe even ten times) larger than predicted.

ACKNOWLEDGEMENTS

We are infinitely grateful to the anonymous referee for her/his thorough comments in greatly improving this manuscript. This research is based on observations made with: (a) the William Herschel Telescope operated on the island of La Palma by the Isaac Newton Group in the Spanish Observatorio del Roque de los Muchachos of the Instituto de Astrofísica de Canarias; (b) ESO Telescopes at the La Silla Paranal Observatory; (c) the 5 m Hale Telescope at the Palomar Observatory; and (d) the Keck I Telescope at the W. M. Keck Observatory. We wish to recognize and acknowledge the very significant cultural role and reverence that the summit of Mauna Kea has always had within the indigenous Hawaiian community. We are most fortunate to have the opportunity to conduct observations from this mountain. KML would like to thank Mischa Schirmer for his invaluable help with the data reduction pipeline THELI and the setting/adding of new instruments to it. We have made

use of the SIMBAD database, operated at CDS, Strasbourg, France; of the NASA/IPAC Extragalactic Database (NED) which is operated by the Jet Propulsion Laboratory, California Institute of Technology, under contract with the National Aeronautics and Space Administration; and of data obtained from the Chandra Data Archive and the Chandra Source Catalog. PGJ and KML acknowledge funding from the European Research Council under ERC Consolidator Grant agreement no 647208. MH acknowledges the ESO fellowship program. MAPT acknowledges support via a Ramón y Cajal Fellowship (RYC-2015-17854) and support by the Spanish Ministry of Economy, Industry and Competitiveness under grant AYA2017-83216-P. TPR acknowledges funding from Science and Technology Facilities Council (STFC) as part of the consolidated grant ST/L00075X/1. DJW acknowledges support from an STFC Ernest Rutherford Fellowship.

REFERENCES

- Abbott B. P., et al., 2016a, *Physical Review X*, **6**, 041015
 Abbott B. P., et al., 2016b, *Physical Review Letters*, **116**, 061102
 Bachetti M., et al., 2014, *Nature*, **514**, 202
 Begelman M. C., 2002, *ApJ*, **568**, L97
 Bertin E., 2006, in Gabriel C., Arviset C., Ponz D., Enrique S., eds, *Astronomical Society of the Pacific Conference Series Vol. 351, Astronomical Data Analysis Software and Systems XV*. p. 112
 Bertin E., Arnouts S., 1996, *A&AS*, **117**, 393
 Bertin E., Mellier Y., Radovich M., Missonnier G., Didelon P., Morin B., 2002, in Bohlender D. A., Durand D., Handley T. H., eds, *Astronomical Society of the Pacific Conference Series Vol. 281, Astronomical Data Analysis Software and Systems XI*. p. 228
 Bohlin R. C., Savage B. D., Drake J. F., 1978, *ApJ*, **224**, 132
 Carpano S., Haberl F., Maitra C., Vasilopoulos G., 2018, *Monthly Notices of the Royal Astronomical Society*, **476**, L45
 Casares J., Jonker P. G., 2014, *Space Sci. Rev.*, **183**, 223
 Coatman L., Hewett P. C., Banerji M., Richards G. T., 2016, *MNRAS*, **461**, 647
 Colbert E. J. M., Heckman T. M., Ptak A. F., Strickland D. K., Weaver K. A., 2004, *ApJ*, **602**, 231
 Copperwheat C., Cropper M., Soria R., Wu K., 2005, *MNRAS*, **362**, 79
 Copperwheat C., Cropper M., Soria R., Wu K., 2007, *MNRAS*, **376**, 1407
 Dobrzycki A., Ebeling H., Glotfelty K., Freeman P., Damiani F., Elvis M., Calderwood T., 1999. p. 142
 Drilling J. S., Landolt A. U., 2000, *Normal Stars*. p. 381
 Dubus G., Rutledge R. E., 2002, *MNRAS*, **336**, 901
 Dubus G., Charles P. A., Long K. S., 2004, *A&A*, **425**, 95
 Earnshaw H. M., 2016, *Astronomische Nachrichten*, **337**, 448
 Elias J. H., Frogel J. A., Humphreys R. M., 1985, *ApJS*, **57**, 91
 Fabbiano G., Zezas A., Murray S. S., 2001, *ApJ*, **554**, 1035
 Fabrika S., Ueda Y., Vinokurov A., Sholukhova O., Shidatsu M., 2015, *Nature Physics*, **11**, 551
 Farrell S. A., et al., 2011, *Astronomische Nachrichten*, **332**, 392
 Fitzpatrick E. L., 1999, *Publications of the Astronomical Society of the Pacific*, **111**, 63
 Fraternali F., van Moorsel G., Sancisi R., Oosterloo T., 2002, *AJ*, **123**, 3124
 Fürst F., et al., 2016, *ApJ*, **831**, L14
 Gaia Collaboration et al., 2018, *A&A*, **616**, A1
 Gladstone J. C., Roberts T. P., Done C., 2009, *MNRAS*, **397**, 1836

- Gladstone J. C., Copperwheat C., Heinke C. O., Roberts T. P., Cartwright T. F., Levan A. J., Goad M. R., 2013, *ApJS*, **206**, 14
- Grisé F., Pakull M. W., Soria R., Motch C., 2009, in Rodriguez J., Ferrando P., eds, American Institute of Physics Conference Series Vol. 1126, American Institute of Physics Conference Series. pp 201–203 ([arXiv:0902.4431](https://arxiv.org/abs/0902.4431)), [doi:10.1063/1.3149412](https://doi.org/10.1063/1.3149412)
- Gutiérrez C. M., López-Corredoira M., 2006, in Meurs E. J. A., Fabbiano G., eds, IAU Symposium Vol. 230, Populations of High Energy Sources in Galaxies. pp 310–311, [doi:10.1017/S1743921306008556](https://doi.org/10.1017/S1743921306008556)
- HI4PI Collaboration et al., 2016, *A&A*, **594**, A116
- Heida M., et al., 2014, *MNRAS*, **442**, 1054
- Heida M., et al., 2015a, *MNRAS*, **453**, 3510
- Heida M., Jonker P. G., Torres M. A. P., 2015b, *MNRAS*, **454**, L26
- Heida M., Jonker P. G., Torres M. A. P., Roberts T. P., Walton D. J., Moon D. S., Stern D., Harrison F. A., 2016, *MNRAS*, **459**, 771
- Heida M., et al., 2019, *ApJ*, **883**, L34
- Hu N., et al., 2018, *ApJ*, **854**, 68
- Israel G. L., et al., 2017a, *Science*, **355**, 817
- Israel G. L., et al., 2017b, *MNRAS*, **466**, L48
- Jonker P. G., Torres M. A. P., Fabian A. C., Heida M., Miniutti G., Pooley D., 2010, *MNRAS*, **407**, 645
- Kaaret P., Feng H., Roberts T. P., 2017, *Annual Review of Astronomy and Astrophysics*, **55**, 303
- Kalirai J. S., et al., 2009, Technical report, WFC3 SMOV Proposal 11450: The Photometric Performance and Calibration of WFC3/UVIS
- Kalogera V., Baym G., 1996, *ApJ*, **470**, L61
- Kausch W., et al., 2015, *A&A*, **576**, A78
- King A. R., Davies M. B., Ward M. J., Fabbiano G., Elvis M., 2001, *ApJ*, **552**, L109
- Kiss L. L., Szabó G. M., Bedding T. R., 2006, *MNRAS*, **372**, 1721
- Koromendy J., Ho L. C., 2013, *ARA&A*, **51**, 511
- Langon A., Hauschildt P. H., Ladjal D., Mouhcine M., 2007, *A&A*, **468**, 205
- Lau R. M., et al., 2019, *ApJ*, **878**, 71
- Levesque E. M., Massey P., Olsen K. A. G., Plez B., Josselin E., Maeder A., Meynet G., 2005, *ApJ*, **628**, 973
- Li Z., et al., 2010, *ApJ*, **721**, 1368
- Lin D., Webb N. A., Barret D., 2012, *ApJ*, **756**, 27
- Liu J., 2011, *ApJS*, **192**, 10
- Liu J.-F., Bregman J., Miller J., Kaaret P., 2007, *ApJ*, **661**, 165
- Long K. S., Dodorico S., Charles P. A., Dopita M. A., 1981, *ApJ*, **246**, L61
- López K. M., Heida M., Jonker P. G., Torres M. A. P., Roberts T. P., Walton D. J., Moon D.-S., Harrison F. A., 2017, *MNRAS*, **469**, 671
- López K. M., Jonker P. G., Heida M., Torres M. A. P., Roberts T. P., Walton D. J., Moon D. S., Harrison F. A., 2019, *MNRAS*, **489**, 1249
- Manchado A., et al., 1998, in Fowler A. M., ed., Society of Photo-Optical Instrumentation Engineers (SPIE) Conference Series Vol. 3354, Proc. SPIE. pp 448–455, [doi:10.1117/12.317270](https://doi.org/10.1117/12.317270)
- Markert T. H., Rallis A. D., 1983, *ApJ*, **275**, 571
- Massey P., Evans K. A., 2016, *ApJ*, **826**, 224
- McLean I. S., et al., 2010, in Proc. SPIE. p. 77351E, [doi:10.1117/12.856715](https://doi.org/10.1117/12.856715)
- McLean I. S., et al., 2012, in Proc. SPIE. p. 84460J, [doi:10.1117/12.924794](https://doi.org/10.1117/12.924794)
- McQuinn K. B. W., Skillman E. D., Dolphin A. E., Berg D., Kennicutt R., 2017, *AJ*, **154**, 51
- Merritt D., Schnittman J. D., Komossa S., 2009, *ApJ*, **699**, 1690
- Mezcua M., Roberts T. P., Sutton A. D., Lobanov A. P., 2013, *Monthly Notices of the Royal Astronomical Society*, **436**, 3128
- Mineo S., Gilfanov M., Sunyaev R., 2012, *MNRAS*, **419**, 2095
- Moon D.-S., Eikenberry S. S., Wasserman I. M., 2003, *ApJ*, **586**, 1280
- Moorwood A., Cuby J.-G., Lidman C., 1998, *The Messenger*, **91**, 9
- Motch C., Pakull M. W., Grisé F., Soria R., 2011, *Astronomische Nachrichten*, **332**, 367
- Motch C., Pakull M. W., Soria R., Grisé F., Pietrzyński G., 2014, *Nature*, **514**, 198
- Mucciarelli P., Zampieri L., Falomo R., Turolla R., Treves A., 2005, *ApJ*, **633**, L101
- Osterbrock D. E., 1989, Astrophysics of gaseous nebulae and active galactic nuclei
- Pakull M. W., Grisé F., 2008, in Bandyopadhyay R. M., Wachter S., Gelino D., Gelino C. R., eds, American Institute of Physics Conference Series Vol. 1010, A Population Explosion: The Nature & Evolution of X-ray Binaries in Diverse Environments. pp 303–307 ([arXiv:0803.4345](https://arxiv.org/abs/0803.4345)), [doi:10.1063/1.2945062](https://doi.org/10.1063/1.2945062)
- Pakull M. W., Grisé F., Motch C., 2006, in Meurs E. J. A., Fabbiano G., eds, IAU Symposium Vol. 230, Populations of High Energy Sources in Galaxies. pp 293–297 ([arXiv:astro-ph/0603771](https://arxiv.org/abs/astro-ph/0603771)), [doi:10.1017/S1743921306008489](https://doi.org/10.1017/S1743921306008489)
- Patruno A., Zampieri L., 2008, *MNRAS*, **386**, 543
- Poutanen J., Fabrika S., Valeev A. F., Sholukhova O., Greiner J., 2013, *MNRAS*, **432**, 506
- Ptak A., Colbert E., van der Marel R. P., Roye E., Heckman T., Towne B., 2006, *ApJS*, **166**, 154
- Qiu Y., et al., 2019, *The Astrophysical Journal*, **877**, 57
- Ramsey C. J., Williams R. M., Gruendl R. A., Chen C.-H. R., Chu Y.-H., Wang Q. D., 2006, *ApJ*, **641**, 241
- Roberts T. P., Warwick R. S., Ward M. J., Murray S. S., 2002, *MNRAS*, **337**, 677
- Roberts T. P., Gladstone J. C., Goulding A. D., Swinbank A. M., Ward M. J., Goad M. R., Levan A. J., 2011, *Astronomische Nachrichten*, **332**, 398
- Rodríguez Castillo G. A., et al., 2019, arXiv e-prints, [p. arXiv:1906.04791](https://arxiv.org/abs/1906.04791)
- Sathyaprakash R., et al., 2019, *MNRAS*, **488**, L35
- Schirmer M., 2013, *ApJS*, **209**, 21
- Shortridge K., 1993, in Hanisch R. J., Brissenden R. J. V., Barnes J., eds, Astronomical Society of the Pacific Conference Series Vol. 52, Astronomical Data Analysis Software and Systems II. p. 219
- Sirianni M., et al., 2005, *PASP*, **117**, 1049
- Skrutskie M. F., et al., 2006, *AJ*, **131**, 1163
- Smette A., et al., 2015, *A&A*, **576**, A77
- Stocke J. T., Wang Q. D., Perlman E. S., Donahue M. E., Schachter J. F., 1995, *AJ*, **109**, 1199
- Swartz D. A., Ghosh K. K., Tennant A. F., Wu K., 2004, *ApJS*, **154**, 519
- The LIGO Scientific Collaboration et al., 2018, arXiv e-prints, [p. arXiv:1811.12907](https://arxiv.org/abs/1811.12907)
- Tikhonov N. A., Lebedev V. S., Galazutdinova O. A., 2015, *Astronomy Letters*, **41**, 239
- Tully R. B., et al., 2013, *AJ*, **146**, 86
- Vinokurov A., Fabrika S., Atapin K., 2018, *The Astrophysical Journal*, **854**, 176
- Wang S., Liu J., Qiu Y., Bai Y., Yang H., Guo J., Zhang P., 2016, *The Astrophysical Journal Supplement Series*, **224**, 40
- Wenger M., et al., 2000, *A&AS*, **143**, 9
- Wiktorowicz G., Sobolewska M., Lasota J.-P., Belczynski K., 2017, *ApJ*, **846**, 17
- Yuan H. B., Liu X. W., Xiang M. S., 2013, *Monthly Notices of the Royal Astronomical Society*, **430**, 2188
- Zampieri L., Roberts T. P., 2009, *Monthly Notices of the Royal Astronomical Society*, **400**, 677
- Zampieri L., Mucciarelli P., Falomo R., Kaaret P., Di Stefano R., Turolla R., Chierigato M., Treves A., 2004, *ApJ*, **603**, 523

APPENDIX A: IMAGES

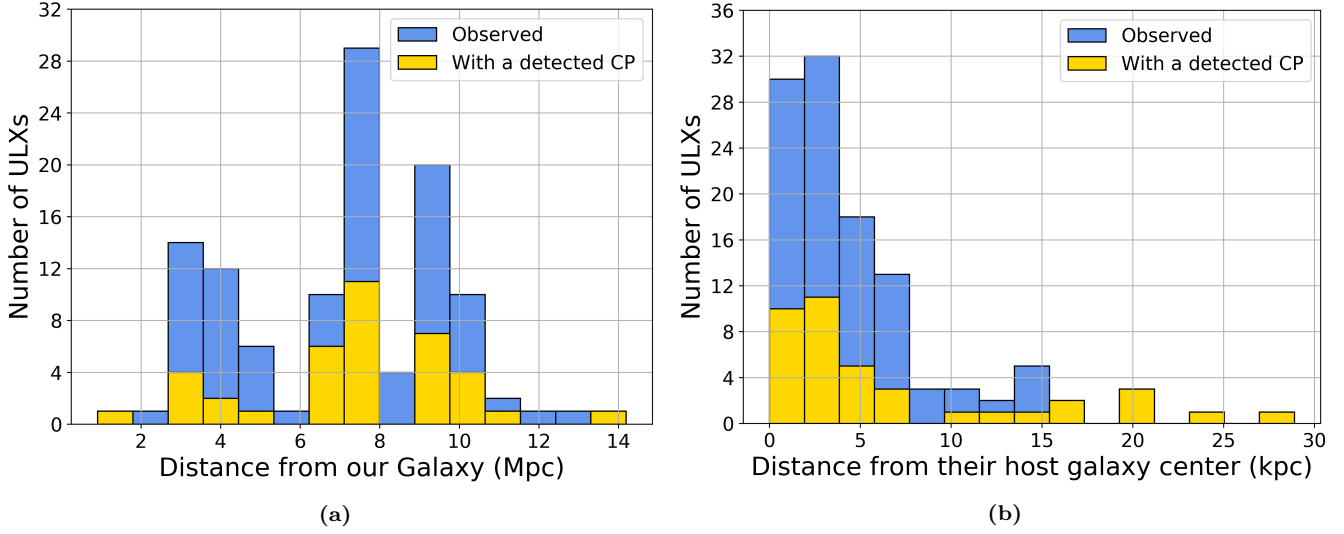


Figure A1. (a) Histogram of the distribution of distances from our Galaxy to the 113 observed ULXs (in blue) and to the 38 ULXs for which we detected a NIR candidate counterpart (in yellow). A K–S test between both distributions reveals that they are not different. (b) Histogram of the distribution of distances to the 113 observed ULXs (in blue) and to the 38 ULXs for which we detected a NIR candidate counterpart (in yellow) from the centre of their respective host galaxies. A K–S test between both distributions reveals that they are not different.

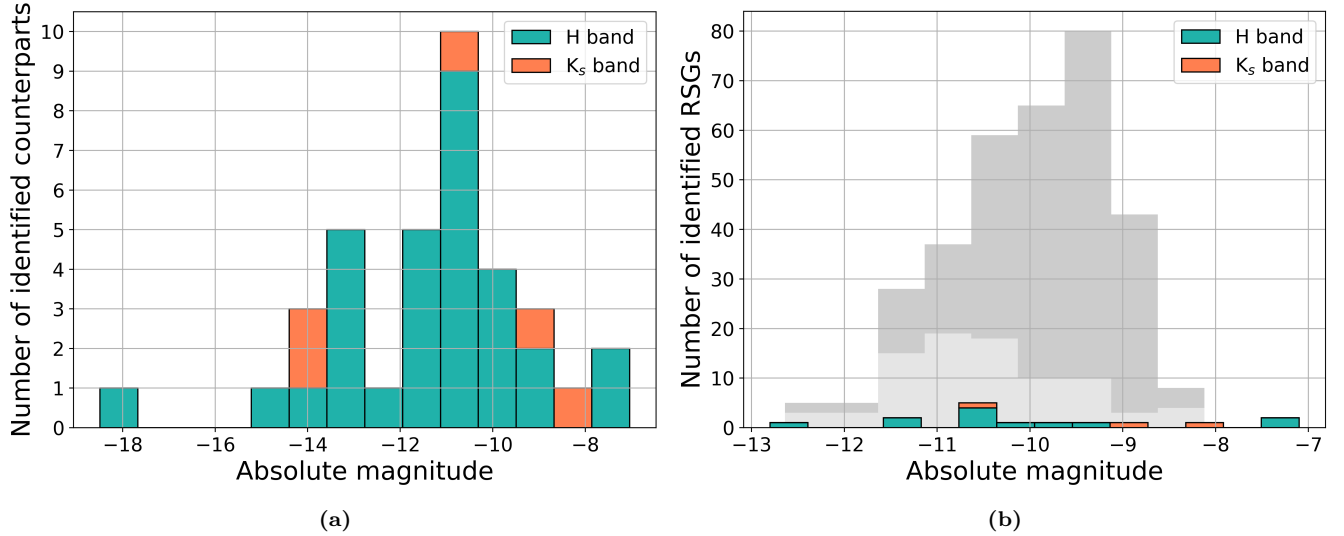


Figure A2. Histogram of the distribution of absolute magnitudes of (a) the detected NIR candidate counterparts, indicating in which band they were observed and detected; and (b) the detected (candidates or confirmed) RSGs counterparts compared with the RSGs present in the MW and LMC (light grey), and in M31 (dark grey).

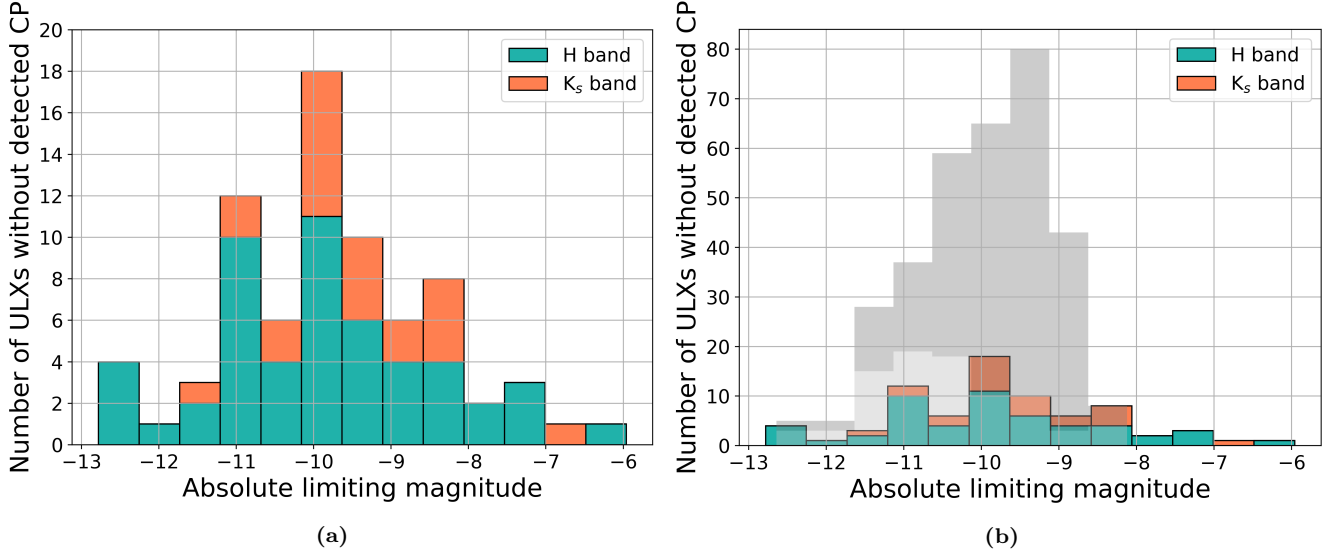


Figure A3. (a) Histogram of the distribution of limiting absolute magnitudes at the position of the ULXs for which we did not detect any counterpart, indicating in which band they were observed. (b) Same as (a) but compared with a histogram of the distribution of absolute magnitudes of the RSGs in the MW and LMC (light grey), and in M31 (dark grey).

APPENDIX B: TABLES

This paper has been typeset from a \TeX/L\AA\TeX file prepared by the author.

Table B1. Updated coordinates for the NIR candidate counterparts detected by Heida et al. (2014) and López et al. (2017), as they used 2MASS sources for the astrometric correction of their NIR images.. We improved the astrometry on those NIR images by finding a local solution around the position of the ULXs using isolated Gaia DR2 sources. We used point sources with a proper motion $\text{pm} < 5 \text{ mas yr}^{-1}$, and, if necessary (i.e. not sufficient sources satisfying that constraint), $\text{pm} < 10 \text{ mas yr}^{-1}$.

Galaxy	ULX name (in SIMBAD)	R.A. (hh:mm:ss)	Dec. (dd:mm:ss)	3- σ positional uncertainty (")
NGC 253	RX J004722.4 – 252051	00:47:22.6	–25:20:51.3	1.5
NGC 925	[SST2011] J022721.52 + 333500.7	02:27:21.5	+33:35:00.7	1.7
NGC 925	[SST2011] J022727.53 + 333443.0	02:27:27.6	+33:34:43.4	1.7
NGC 1058	XMMU J024323.5 + 372038	02:43:23.4	+37:20:42.3	1.5
NGC 1637	[IWL2003 68]	04:41:32.9	–02:51:26.3	2.0
NGC 2403	RX J073655.7 + 653542	07:36:55.4	+65:35:41.6	0.7
NGC 2500	CXO J080157.8 + 504339	08:01:57.9	+50:43:39.1	1.4
Holmberg I	[WMR2006] Ho I XMM1	09:41:30.2	+71:12:35.6	0.6
Holmberg II	Holmberg II X-1	08:19:29.0	+70:42:19.1	1.3
NGC 3521	[SST2011] J110545.62 + 000016.2	11:05:45.6	+00:00:17.5	0.4
NGC 3627	[SST2011] J112018.32 + 125900.8	11:20:18.3	+12:59:01.2	1.1
NGC 4136	CXOU J120922.6 + 295551	12:09:22.6	+29:55:50.5	1.8
NGC 4136	[SST2011] J120922.18 + 295559.7	12:09:22.1	+29:55:59.0	1.5
NGC 4258	RX J121844.0 + 471730	12:18:43.9	+47:17:31.9	1.3
NGC 4258	3XMM J121847.6 + 472054	12:18:47.7	+47:20:52.8	3.9
NGC 4258	[LB2005] NGC 4258 X9	12:19:23.3	+47:09:40.7	1.1
NGC 4485	RX J1230.5 + 4141	12:30:30.4	+41:41:42.7	0.6
NGC 4490	[SST2011] J123029.55 + 413927.6	12:30:29.6	+41:49:27.0	0.6
NGC 4490	CXO J123038.4 + 413831	12:30:38.2	+41:38:31.5	0.6
NGC 4490	2XMM J123043.1 + 413819	12:30:43.1	+41:38:19.2	0.6
NGC 4559	[SST2011] J123557.79 + 275807.4	12:35:57.7	+27:58:08.0	1.5
		12:35:57.8	+27:58:07.2	1.5
NGC 4559	RX J123558 + 27577	12:35:58.6	+27:57:41.7	1.5
NGC 4594	[LB2005] NGC 4594 X5	12:40:22.7	–11:39:24.8	0.5
NGC 4631	[SST2011] J124211.13 + 323235.9	12:43:11.2	+32:32:36.7	1.0
NGC 5194	XMMU J132953.3 + 471040	13:29:53.3	+47:10:42.9	2.5
NGC 5194	RX J132947 + 47096	13:29:47.5	+47:09:40.8	0.8
NGC 5408	NGC 5408 X-1	14:03:19.7	–41:22:58.7	2.1
NGC 5457	2E 1402.4 + 5440	14:04:14.3	+54:26:02.4	1.4
NGC 5457	2XMM J140248.0 + 541350	14:02:48.2	+54:13:50.4	1.3
NGC 5457	CXOU J140314.3 + 541807	14:03:14.4	+54:18:07.2	1.4
NGC 5457	[LB2005] NGC 5457 X32	14:02:28.2	+54:16:26.3	0.8
NGC 5457	[LB2005] NGC 5457 X26	14:04:29.2	+54:23:53.4	0.7